Cosmological tensions in Proca-Nuevo theory

Hsu-Wen Chiang,^a Claudia de Rham,^{b,c,d} Sebastian Garcia-Saenz,^a Xue Zhou^a

- ^aDepartment of Physics, Southern University of Science and Technology, Shenzhen 518055, China
- ^bAbdus Salam Centre for Theoretical Physics, Imperial College, London, SW7 2AZ, UK
- $^c\mathrm{CERCA},$ Department of Physics, Case Western Reserve University, 10900 Euclid Ave, Cleveland, OH 44106, USA
- $^d\mathrm{Perimeter}$ Institute for Theoretical Physics, 31 Caroline St N, Waterloo, ON N2L 2Y5, Canada

E-mail: jiangxw[at]sustech.edu.cn, b98202036[at]ntu.edu.tw, c.de-rham[at]imperial.ac.uk, sgarciasaenz[at]sustech.edu.cn, 12332935[at]mail.sustech.edu.cn

Abstract. We study the cosmological predictions of (extended) Proca-Nuevo theory. This vector-tensor theory enjoys stable homogeneous and isotropic solutions characterized by an effective dark energy fluid, with behavior that ranges from freezing quintessential to thawing phantom-like, serving as a motivated framework to scrutinize the cosmological tensions that affect the standard Λ CDM model. While the model we consider is sufficiently generic to encompass a large class of field theories, it distinguishes itself from scalar dark energy models (quintessential ones, kinetic ones and non-minimally coupled ones) by the presence of what would be classed as a vector degree of freedom which can be for instance inherited from more generic theories of gravity. We improve on previous work in several directions: we consider a general one-parameter class of background models; identify a so-called 'special' model and analyze observational constraints taking also into account perturbations and making use of wide up-to-date catalogs of datasets including recently released ones. We find that the oneparameter Proca-Nuevo model is preferred over Λ CDM at 1.5 σ when fitting CMB and BAO data, and at 2.4σ when further adding low-redshift data. The Hubble tension is alleviated, dropping from 5.8σ to 2.3σ (resp. 1.5σ) between CMB with (and resp. without) BAO data and local measurements. On the other hand, we find that the vector field generically introduces a significant enhancement of the effective Newton constant, so that matching the observed matter power spectrum requires a mild amount of tuning to suppress the impact of perturbations. Since, at the background level, Proca-Nuevo is degenerate with other classes of theories, our results are also relevant to a wider range of set-ups including and beyond vector-tensor models.

Co	ontents	
1	Introduction	1
2	Set-up	3
	2.1 Extended Proca-Nuevo	4
	2.2 Cosmological backgrounds	5
	2.3 Special and very special EPN models	7
	2.4 General EPN model	Ĉ
	2.5 Linear perturbations in the special EPN model	10
3	Data and analysis methodology	12
4	Results	15
	4.1 Parameter constraints	15
	4.2 Matter power spectrum and structure growth	19
	4.3 Model comparison	22
5	Conclusions	2 5
\mathbf{A}	Initial conditions, effective Newton constant, and anisotropic stress	2 6
	A.1 Adiabatic initial conditions	26
	A.2 Effective Newton constant and anisotropic stress	28
В	Information Criteria	29
\mathbf{C}	Full constraint plot of cosmological parameters	30

1 Introduction

The resolution of observational tensions in cosmological data has emerged as a major challenge in the current area of precision cosmology. Whether the resolution will lie within systematics, or truly points towards signs of new physics is yet unclear but explorations along all directions have been flourishing. Prime among these is the "Hubble tension", the 5.3σ difference in the measurements of the Hubble constant H_0 from cosmic microwave background (CMB) data by the Planck satellite [1] and local observations of Cepheids and SNe type Ia distance ladder by the SH0ES collaboration [2]. In addition, a slightly less pronounced but still relevant tension occurs in the $\Omega_{\rm m0}-S_8$ parameter space, with $\Omega_{\rm m0}=0.3158\pm0.0064$ and $S_8=0.829\pm0.011$ from the CMB dataset of Planck [1, 3, 4], $\Omega_{\rm m0}=0.2962\pm0.0095$ and $S_8=0.836\pm0.035$ from the galaxy clustering dataset of DESI [5], and $\Omega_{\rm m0}=0.280^{+0.037}_{-0.046}$ and $S_8=0.790^{+0.018}_{-0.014}$ from the galaxy weak lensing dataset of DES Y3 + KiDS-1000 [6], each in weak tension with each other.

Cosmological tensions are threatening the decades-long reign of the Λ CDM model. If confirmed, a likely suspect would be the least understood ingredient in the model, i.e. the

 $^{^{1}\}Omega_{\rm m0}$ is the matter density parameter, with the subscript "0" denoting quantities evaluated at the present time; $S_{8} \equiv \sigma_{8} \sqrt{\Omega_{\rm m0}/0.3}$ measures the matter spectrum's power, with σ_{8} the root-mean-square of matter fluctuations at the scale of $8 \,\mathrm{Mpc}/h$; $h \equiv H_{0}/(100 \,\mathrm{km \ s^{-1} \ Mpc^{-1}})$ is the rescaled Hubble constant.

cosmological constant. In fact, even before any anomaly had emerged, cosmologists have long entertained the possibility that a dynamical field might be a more natural explanation for dark energy. It has nevertheless proved challenging to devise well-motivated models that match the successes of Λ CDM while resolving the tensions, since any modification to the Hubble expansion inevitably alters multiple predictions, often leading to unexpected conflicts; see [7–13] for reviews. This aspect has motivated more minimal approaches based on phenomenological models, such as the Chevallier-Polarski-Linder (CPL) parametrization of the dark energy equation of state: $w_{\rm DE} = w_0 + (1-a)w_a$. A remarkable finding is that recent data appear to potentially indicate an evolving dark energy, which if confirmed would challenge standard minimally coupled models of quintessence, [14]. In addition, recent data also favor $w_{\rm DE} < -1$ [15] (see however [16–18]), which for matter minimally coupled to standard Einstein gravity would violate the null energy condition. It is well known that crossing this "phantom divide" can easily lead to catastrophic consequences [19, 20], underscoring the need for a deeper understanding of how such behavior might emerge within consistent theoretical frameworks.

A conceptually minimal description of evolving dark energy is given by a scalar field condensate, as in the well-studied quintessence scenario [21]. However, the aforementioned issues with phantom-like behavior indicate that other classes of models may be better motivated, including Galileons with broken shift symmetry [22]. Of similar nature, another class of models that has emerged as particularly compelling is the vector-tensor class of gravitational theories, specifically the models that include non-trivial interactions, such as derivative self-couplings or non-minimal gravitational couplings, thus generalizing the Proca theory of a massive vector field. This program, starting with the discovery of the so-called Generalized Proca (GP) theory [23–25], has led to a wealth of interesting results of phenomenological interest in astrophysics (e.g. hairy black holes [26–28] and destabilization mechanisms [29–33]) and cosmology [34–39], including in particular the possibility to address the Hubble tension [40, 41]. Importantly, these models have been shown to be theoretically robust, including a consistent constraint structure [42].

An interesting member of the generalized vector-tensor class of theories is the so-called Proca-Nuevo (PN) [43], or its extended version (EPN) [44]. Several aspects motivate us to study these models in connection with the issue of cosmological tensions. The first is that the theory is characterized by cosmological solutions with an effective dark energy fluid, without the need of a cosmological constant, and this fluid may exhibit both phantom-like and 'freezing' ($\dot{w}_{\rm DE} < 0$) quintessence behaviors. Although this is similar to scalar-tensor models, it should be noted that these features emerge from derivative-type interactions rather than from unusual potentials and may therefore be seen as more natural and robust from a fundamental perspective. Indeed, additional graviton polarizations can in some limit be mimicked by what would be classed as additional scalar and vector degrees of freedom for cosmological purposes and by their very nature, enter with specific classes of derivative interactions and non-minimal coupling to the tensor mode (what can be identified as the standard gravitational part). Such features appear in generic theoretically motivated models of gravity, including those with extra dimensions [45] and finite range gravity [46] including massive gravity [47–49].

An advantage of such models is that the hierarchy between the scale of dark energy (encoded for instance in the graviton mass) and the Planck scale is protected by a non-renormalization theorem, see for instance [50–52] for the quantum stability of these models and theoretical consistency against their embedding in a standard and healthy UV completion. This implies that these classes of models are technically natural in the sense that one would

not expect quantum corrections to destabilize the system. As a small comment, we may note when comparing with cosmological observations, data favor a relatively large mass of the vector field of about two orders of magnitude larger that the Hubble parameter today. If we were to relate this back to a model of massive gravity, this would correspond to a graviton mass of the order of $\mathcal{O}\left(10^{-31}\text{eV}\right)$ which is still well within the acceptable range, both observationally [53] and theoretically [54, 55].

Importantly, the effective phantom behavior need only be transient and does not necessarily give rise to instabilities at the level of perturbations in more general models (e.g. see also [22, 56]). In what follows we shall focus our analysis on the EPN class of models. Although EPN is inequivalent to GP, it includes a subset of it and also accommodates a greater number of free functions. This allows for both a more general behavior at the phenomenological level and the possibility that specific choices of coefficients could yield particularly simple models. Indeed, the EPN class includes a so-called 'special' model, which boasts interesting features such as a minimal set of free functions and the absence of non-minimal interactions with gravity. In fact, for a natural choice of coefficients, the model leads to a background evolution characterized by the same number of parameters as Λ CDM. Finally, we note that previous studies of the cosmological predictions of EPN have revealed very promising results, providing a very good fit to late-time data in the case of the no-parameter model just mentioned [57, 58].

These considerations prompt us to revisit the question of confronting EPN with data. As mentioned, previous work was restricted to a particular member of this class of theories and focused exclusively on low-redshift data. We extend this line of investigation in three directions: we consider a more general subclass of models, leading to a one-parameter modification of the Friedmann equation; restricted to this 'special' model, we take into account observational constraints also at the level of perturbations; our analysis makes use of a more complete set of newly released state-of-the-art datasets, including early- and late-universe measurements. Specifically, regarding the last point, we utilize data from *Planck* 2018 low- ℓ CMB TTEE [3], NPIPE PR4 *Planck* CamSpec high- ℓ CMB TTTEEE [1], NPIPE PR4 *Planck* CMB lensing [4, 65], DESI DR1 BAO [15, 66, 67], Pantheon+ SNe Type Ia [68], SH0ES local H_0 measurements [2], SDSS DR16, SDSS DR7 and 6dF galaxy clustering datasets [69–71]. In particular, the inclusion of the *Planck* dataset enables us to analyze the pros and cons of EPN theory more comprehensively and to establish a more informed comparison against other set-ups.

The paper is structured as follows. Sec. 2 presents a review of cosmology in EPN theory, both at the homogeneous and isotropic background level and, in the case of the special EPN model, for linear perturbations. In Sec. 3 we detail the analysis methodology, the astrophysical and cosmological datasets, and the information criteria used in this work. Sec. 4 presents our results of parameter posterior, CMB and matter power spectrum, structure growth, and the tension analysis. Here we also discuss the comparison between the results of EPN and other dark energy candidate models. We summarize and offer final remarks in Sec. 5.

2 Set-up

In this section we present a concise review of EPN theory and its predictions in the context of FLRW cosmology. After general discussions of the theory in Sec. 2.1 and the background equations of motion in Sec. 2.2, we turn our attention to the so-called 'special' EPN, a

²See also [59–61] for other studies of cosmological aspects of GP theory and [62–64] for EPN.

distinguished subclass of models characterized by the absence of non-minimal couplings with gravity. We show in Sec. 2.3 how a particular choice of free functions leads to a one-parameter modification of the Friedmann equation. In Sec. 2.4 we also point out that some particular instances of this one-parameter class may obtained more naturally from the general EPN model. Finally, in Sec. 2.5 we review and generalize the analysis of linear perturbations in the special EPN model, extending the results of [44] to the one-parameter deformation mentioned above.

2.1 Extended Proca-Nuevo

Extended Proca-Nuevo (EPN) is a non-linear vector-tensor theory describing a massive spin-1 field A_{μ} coupled to gravity. The full action, including also the Einstein-Hilbert term and standard matter, is given by

$$S = \int d^4x \sqrt{-g} \left(\frac{M_{\rm Pl}^2}{2} R + \mathcal{L}_{\rm EPN} + \mathcal{L}_{\rm M} \right) , \qquad (2.1)$$

where $M_{\rm Pl}$ is the reduced Planck mass and

$$\mathcal{L}_{EPN} = -\frac{1}{4} F^{\mu\nu} F_{\mu\nu} + \Lambda^4 \left(\hat{\mathcal{L}}_0 + \hat{\mathcal{L}}_1 + \hat{\mathcal{L}}_2 + \hat{\mathcal{L}}_3 \right) , \qquad (2.2)$$

is the EPN Lagrangian [43, 44]. The latter is a function of the field strength $F_{\mu\nu} = \nabla_{\mu}A_{\nu} - \nabla_{\nu}A_{\mu}$ and

$$\hat{\mathcal{L}}_{0} = \alpha_{0}(X),$$

$$\hat{\mathcal{L}}_{1} = \alpha_{1}(X)\mathcal{L}_{1}[\mathcal{K}] + d_{1}(X)\frac{\mathcal{L}_{1}[\nabla A]}{\Lambda^{2}},$$

$$\hat{\mathcal{L}}_{2} = (\alpha_{2}(X) + d_{2}(X))\frac{R}{\Lambda^{2}} + \alpha_{2,X}(X)\mathcal{L}_{2}[\mathcal{K}] + d_{2,X}(X)\frac{\mathcal{L}_{2}[\nabla A]}{\Lambda^{4}},$$

$$\hat{\mathcal{L}}_{3} = \left(\alpha_{3}(X)\mathcal{K}^{\mu\nu} + d_{3}(X)\frac{\nabla^{\mu}A^{\nu}}{\Lambda^{2}}\right)\frac{G_{\mu\nu}}{\Lambda^{2}} - \frac{1}{6}\alpha_{3,X}(X)\mathcal{L}_{3}[\mathcal{K}] - \frac{1}{6}d_{3,X}(X)\frac{\mathcal{L}_{3}[\nabla A]}{\Lambda^{6}},$$
(2.3)

which are constructed out of the matrices $\mathcal{K}^{\mu}{}_{\nu} \equiv \left(\sqrt{g^{-1}f[A]}\right)^{\mu}{}_{\nu} - \delta^{\mu}_{\nu}$ and $(\nabla A)^{\mu}{}_{\nu} \equiv g^{\mu\alpha}\nabla_{\alpha}A_{\nu}$. Here

$$f_{\mu\nu}[A] = g_{\mu\nu} + 2\frac{\nabla_{(\mu}A_{\nu)}}{\Lambda^2} + \frac{\nabla_{\mu}A_{\alpha}g^{\alpha\beta}\nabla_{\nu}A_{\beta}}{\Lambda^4}, \qquad (2.4)$$

and

$$\mathcal{L}_n[M] = -\frac{1}{(4-n)!} \epsilon^{\mu_1 \dots \mu_4} \epsilon_{\nu_1 \dots \nu_4} M^{\nu_1}{}_{\mu_1} \dots M^{\nu_n}{}_{\mu_n} \delta^{\nu_{n+1}}{}_{\mu_{n+1}} \dots \delta^{\nu_4}{}_{\mu_4}, \qquad (2.5)$$

for any matrix M. We have also introduced in (2.3) the scalar

$$X \equiv -\frac{1}{2\Lambda^2} A_\mu A^\mu \,, \tag{2.6}$$

and Λ denoting an energy scale controlling the strength of non-linearity in the theory. The EPN terms (2.3) involve non-minimal gravitational couplings with the curvature scalar R and Einstein tensor $G_{\mu\nu}$, as well as a set of arbitrary functions $\alpha_n(X)$ and $d_n(X)$ (with the notation $\alpha_{n,X} \equiv \frac{\partial}{\partial X} \alpha_n$).

The operators proportional to the functions d_n are part of the GP class [23, 24], while the ones proportional to the functions α_n are the PN terms [43]. EPN theory, which combines these two models, provides a consistent, fully non-linear (in fact, non-polynomial) completion of the minimally coupled Proca theory of a massive vector field. From the viewpoint of degree of freedom count, the theory is described by massive spin-1 and massless spin-2 fields up to the Planck scale and thus provides a predictive framework that captures both non-linear and gravitational effects.

A nice consequence of the combination of GP and PN operators in EPN theory is the possibility of tuning the coefficient functions so as to remove the non-minimal couplings with gravity. Indeed, setting $\alpha_2 + d_2 = 0$, and $\alpha_3 + d_3 = 0$, we arrive at

$$\hat{\mathcal{L}}_{0}^{s} = \alpha_{0}(X) ,$$

$$\hat{\mathcal{L}}_{1}^{s} = \alpha_{1}(X)\mathcal{L}_{1}[\mathcal{K}] + d_{1}(X)\frac{\mathcal{L}_{1}[\nabla A]}{\Lambda^{2}} ,$$

$$\hat{\mathcal{L}}_{2}^{s} = \alpha_{2,X}(X) \left(\mathcal{L}_{2}[\mathcal{K}] - \frac{\mathcal{L}_{2}[\nabla A]}{\Lambda^{4}}\right) ,$$

$$\hat{\mathcal{L}}_{3}^{s} = -\frac{1}{6}\alpha_{3,X}(X) \left(\mathcal{L}_{3}[\mathcal{K}] - \frac{\mathcal{L}_{3}[\nabla A]}{\Lambda^{6}}\right) ,$$
(2.7)

which we will refer to as the 'special' EPN theory.

2.2 Cosmological backgrounds

In this work we focus on a flat Friedmann-Lemaître-Robertson-Walker (FLRW) background

$$g_{\mu\nu}\mathrm{d}x^{\mu}\mathrm{d}x^{\nu} = -\mathrm{d}t^2 + a^2(t)\delta_{ij}\mathrm{d}x^i\mathrm{d}x^j\,,\tag{2.8}$$

with scale factor a(t). Homogeneity and isotropy dictate that the vector field must have the form

$$A_{\mu} \mathrm{d}x^{\mu} = -\phi(t)\mathrm{d}t\,,\tag{2.9}$$

in terms of a scalar function ϕ . Variation of the action (2.1) yields the following equations of motion:

$$H^{2} = \frac{1}{3M_{\rm Pl}^{2}} \left(\rho_{\rm M} + \rho_{\rm EPN} \right) , \qquad (2.10)$$

$$\dot{H} + H^2 = -\frac{1}{6M_{\rm Pl}^2} \left(\rho_{\rm M} + \rho_{\rm EPN} + 3P_{\rm M} + 3P_{\rm EPN} \right) , \qquad (2.11)$$

$$0 = \alpha_{0,X} + 3 \left(\alpha_{1,X} + d_{1,X}\right) \frac{H\phi}{\Lambda^2} + 6 \left[\left(\alpha_{2,X} + d_{2,X}\right) + \left(\alpha_{2,XX} + d_{2,XX}\right) \frac{\phi^2}{\Lambda^2} \right] \frac{H^2}{\Lambda^2} - \left[3 \left(\alpha_{3,X} + d_{3,X}\right) + \left(\alpha_{3,XX} + d_{3,XX}\right) \frac{\phi^2}{\Lambda^2} \right] \frac{H^3\phi}{\Lambda^4},$$
(2.12)

where the first two correspond to the Friedmann and Raychaudhuri equations, respectively, while (2.12) is obtained from the vector field equation. The fact that the latter is a constraint, rather than an evolution equation for ϕ , is a consequence of the peculiar structure of the EPN Lagrangian. Here $H = \dot{a}/a$ is the Hubble parameter, with the overscript dot denoting the

time derivative, and $\rho_{\rm M}$, $P_{\rm M}$, $\rho_{\rm EPN}$ and $P_{\rm EPN}$ are the effective fluid density and pressure from the matter and EPN Lagrangians, respectively, with

$$\rho_{\text{EPN}} = \Lambda^{4} \left\{ -\alpha_{0} + \alpha_{0,X} \frac{\phi^{2}}{\Lambda^{2}} + 3\left(\alpha_{1,X} + d_{1,X}\right) \frac{H\phi^{3}}{\Lambda^{4}} \right.$$

$$+ 6 \left[-\left(\alpha_{2} + d_{2}\right) + 2\left(\alpha_{2,X} + d_{2,X}\right) \frac{\phi^{2}}{\Lambda^{2}} + \left(\alpha_{2,XX} + d_{2,XX}\right) \frac{\phi^{4}}{\Lambda^{4}} \right] \frac{H^{2}}{\Lambda^{2}} \right.$$

$$- \left[5\left(\alpha_{3,X} + d_{3,X}\right) + \left(\alpha_{3,XX} + d_{3,XX}\right) \frac{\phi^{2}}{\Lambda^{2}} \right] \frac{H^{3}\phi^{3}}{\Lambda^{6}} \right\},$$

$$P_{\text{EPN}} = \Lambda^{4} \left\{ \alpha_{0} - \left(\alpha_{1,X} + d_{1,X}\right) \frac{\phi^{2}\dot{\phi}}{\Lambda^{4}} + 2\left(\alpha_{2} + d_{2}\right) \frac{3H^{2} + 2\dot{H}}{\Lambda^{2}} \right.$$

$$- 2\left(\alpha_{2,X} + d_{2,X}\right) \frac{\phi\left(3H^{2}\phi + 2H\dot{\phi} + 2\dot{H}\phi\right)}{\Lambda^{4}} - 4\left(\alpha_{2,XX} + d_{2,XX}\right) \frac{H\phi^{3}\dot{\phi}}{\Lambda^{6}} + \left[\left(\alpha_{3,X} + d_{3,X}\right) \frac{2H^{2}\phi + 3H\dot{\phi} + 2\dot{H}\phi}{\Lambda^{3}} + \left(\alpha_{3,XX} + d_{3,XX}\right) \frac{H\phi^{2}\dot{\phi}}{\Lambda^{5}} \right] \frac{H\phi^{2}}{\Lambda^{3}} \right\}.$$

For the sake of concreteness, we specify at this stage the functions $\alpha_n(X)$ and $d_n(X)$ as follows:

$$\alpha_{1} = -b_{1}\tilde{X}^{p_{1}} - c_{1}\tilde{X}, \quad \alpha_{2} = \frac{b_{2}}{3}\tilde{X}^{2}X + \frac{c_{2}}{2}\tilde{X}X, \quad \alpha_{3,X} = b_{3}\tilde{X}^{2} + c_{3}\tilde{X}, \quad \alpha_{0} = -c_{m}\tilde{X}^{p_{0}},$$

$$d_{1} = -e_{1}\tilde{X}^{p_{1}} + c_{1}\tilde{X}, \quad d_{2} = \frac{e_{2}}{3}\tilde{X}^{2}X - \frac{c_{2}}{2}\tilde{X}X, \quad d_{3,X} = e_{3}\tilde{X}^{2} - c_{3}\tilde{X}, \quad (2.15)$$

where $\tilde{X} \equiv M_{\rm Pl}^{-2} \Lambda^2 X$ and b_n , c_n , e_n , p_n and c_m are constants, left arbitrary for the time being. We remark that, in the case $p_0 = 1$, c_m is actually fixed in terms of the mass of the vector particle when considering the theory on Minkowski space ($\phi = 0$):

$$m^2 \equiv \frac{\Lambda^4 c_m}{M_{\rm Pl}^2} \,. \tag{2.16}$$

The constraint equation and effective density can then be expressed as

$$p_{0}c_{m}\left(\frac{\phi^{2}}{2M_{\rm Pl}^{2}}\right)^{p_{0}} = -3p_{1}(b_{1} + e_{1})\frac{H\phi}{\Lambda^{2}}\left(\frac{\phi^{2}}{2M_{\rm Pl}^{2}}\right)^{p_{1}} + \frac{15(b_{2} + e_{2})H^{2}\phi^{6}}{4M_{\rm Pl}^{4}\Lambda^{4}} - \frac{7(b_{3} + e_{3})H^{3}\phi^{7}}{8M_{\rm Pl}^{4}\Lambda^{6}},$$

$$(2.17)$$

$$\frac{\rho_{\rm EPN}}{\Lambda^{4}} = c_{m}\left(\frac{\phi^{2}}{2M_{\rm Pl}^{2}}\right)^{p_{0}} + \frac{5(b_{2} + e_{2})H^{2}\phi^{6}}{4M_{\rm Pl}^{4}\Lambda^{4}} - \frac{(b_{3} + e_{3})H^{3}\phi^{7}}{2M_{\rm Pl}^{4}\Lambda^{6}}.$$

$$(2.18)$$

This parameterization generalizes the model studied in [44] by the inclusion of the powers p_0 and p_1 , and it is analogous to the one employed in [41] in the context of GP theory. Although valid in a phenomenological study, it is clear that not every choice of p_0 and p_1 will correspond to a consistent effective field theory.

It is worth commenting on the similarities and differences between the cosmology in EPN theory and other cosmological models. The key feature, as already mentioned, is the fact that the scalar ϕ satisfies an algebraic equation, as well as the fact that ϕ only enters

algebraically in the Friedmann equation. In principle, then, one may eliminate ϕ algebraically so as to obtained a fully decoupled evolution equation for the scale factor (provided, as usual, that $\rho_{\rm M}$ is known in terms of a). This is in contrast with scalar-tensor theories including quintessence [21] and Horndeski theory [72–76] where the scalar field is dynamical and the equations cannot in general be decoupled (unless a certain global symmetry exists [77]). On the other hand, there exist several other models of dark energy that may be recast into an independent modified Friedmann equation, such as Palatini f(R) [78], f(T) [79, 80] and f(Q) theories [81], holographic dark energy [82], and some braneworld scenarios [45, 83–86]. It is an attractive aspect of EPN theory that this property is achieved in what is arguably a more minimalistic way, in particular without any modification of the gravitational sector, while making explicit the properties of the additional degrees of freedom required to drive the accelerated expansion.

EPN is however not unique in this respect, since GP theory also enjoys an analogous constraint on the vector field [37, 41]. In fact, at the cosmological background level, the constraint of EPN is formally identical to the one of GP, as is clear from the structure of (2.12). The results of our analysis, when restricted to the background dynamics, will therefore be directly applicable to GP theory (and in fact also to more general theories of gravity with non-minimally coupled non-scalar degrees of freedom, as we will remark later). On the other hand, we emphasize that perturbations break this degeneracy, which as already mentioned is an important motivation for taking them into account in our analysis.

2.3 Special and very special EPN models

We recalled in Sec. 2.1 that there exists a choice for the functions $d_2(X)$ and $d_3(X)$ which results in the cancellation of the non-minimal couplings between the vector field and the metric. At the level of the parametrization (2.15), this corresponds to setting $b_2 + e_2 = 0$ and $b_3 + e_3 = 0$. This 'special' model is of particular interest as it guarantees unity of the tensor perturbation propagation speed; deviations from the speed of light are severely constrained by the neutron star binary merger observation [87] at LVK frequencies. Whether those bound apply to models of dark energy as the ones proposed here depends on the cutoff of the effective field theory [88–90].

Even without non-minimal coupling, the effective energy density of the EPN field possesses non-trivial scaling with respect to H,

$$\rho_{\text{EPN}} = c_m \Lambda^4 \left(\frac{3p_1(b_1 + e_1)}{p_0 c_m} \frac{\sqrt{2} M_{\text{Pl}} H}{\Lambda^2} \right)^{2M} = \rho_{\text{EPN},0} \left(\frac{H}{H_0} \right)^{2M} , \qquad (2.19)$$

where

$$M \equiv -\frac{p_0}{(1 - 2p_0 + 2p_1)}, \qquad (2.20)$$

is the scaling parameter of the background cosmic evolution. Here we keep p_0 as a free parameter for the sake of generality but, as explained previously, one would expect a consistent EFT to have $p_0 = 1$ and $p_1 = 2$, corresponding to the particular model discussed and analyzed in [44, 57, 58]. This choice leads to M = -1/3 < 0, hinting at the fundamental phantom nature of EPN. To avoid confusion, we refer to this particular case as 'very special model', while the special model with M kept as adjustable parameter will be called 'special M model'.

³As we discuss in Sec. 3, later we will need to distinguish between models valid only at the background level (neglecting perturbations of the dark energy field) and those which take full account of linear perturbations. The 'very special model' refer to the latter.

We may verify the phantomness property by solving the Friedmann and Raychaudhuri equations, cf. (2.10) and (2.11), in terms of density parameters Ω_i and equations of state parameters w_i ,

$$\Omega_i \equiv \frac{\rho_i}{3M_{\rm Pl}^2 H^2}, \quad w_i \equiv \frac{P_i}{\rho_i}, \quad 1 = \sum_i \Omega_i, \quad \frac{\dot{H}}{H^2} = -\frac{3}{2} \sum_i (1 + w_i) \Omega_i,$$
(2.21)

where i runs over individual components such as baryons, cold dark matter, etc.

For simplicity, let us consider two non-interacting fluids in addition to EPN: radiation 'r' representing photons, neutrino kinetic energy, etc., and pressureless matter 'm' representing baryons, cold dark matter, etc., with the density scaling $\rho_{\rm r} \propto a^{-4}$ and $\rho_{\rm m} \propto a^{-3}$. Then we have

$$\left(\frac{H}{H_0}\right)^2 = \Omega_{\rm m0}(1+z)^3 + \Omega_{\rm r0}(1+z)^4 + \Omega_{\rm EPN0}\left(\frac{H}{H_0}\right)^{2M},\tag{2.22}$$

where z = 1/a(t) - 1 is the redshift (with the scale factor at present time $a_0 \equiv 1$). The effective equation of state of the EPN model $w_{\rm EPN}$ is then inferred to be

$$w_{\rm EPN} = -\frac{1 - M - M\Omega_{\rm r}/3}{1 - M\Omega_{\rm EPN}}.$$
(2.23)

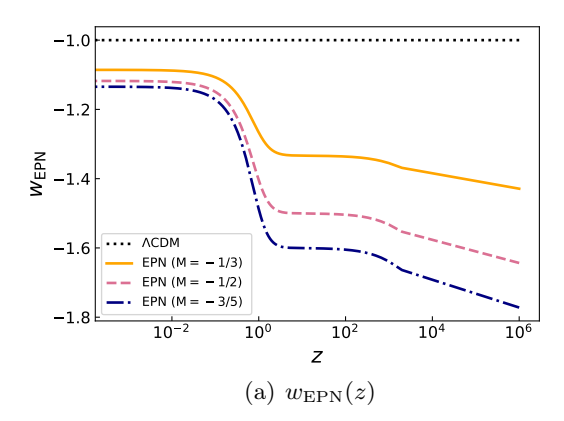
It follows that $w_{\rm EPN} < -1$ if M < 0, equivalently $p_1 \ge p_0 - 1/2$, evincing phantom behavior across broad ranges of EFT setups without relying on non-minimal gravitational interactions to break the null energy condition. This feature makes the special M model particularly interesting and warrants close inspection. On the other hand, for 0 < M < 1/2, i.e. $p_1 \le -1/2$, the system behaves like quintessence, with $-1 < w_{\rm EPN} < -1/3$. It is clear however that $w_{\rm EPN}$ cannot cross the phantom divide w = -1, i.e. the so-called quintom scenario, as illustrated in Fig. 1. Instead it follows a thawing phantom/freezing quintessence trajectory with the tracking behavior

$$w_{\text{EPN}} = \begin{cases} -1 + 4M/3, & \text{in radiation-dominated era,} \\ -1 + M, & \text{in matter-dominated era,} \\ -1, & \text{in dark-energy-dominated era.} \end{cases}$$
 (2.24)

This aspect motivates the investigation of more general parameterizations in future work. The EPN equation of state also constrains the scaling of the condensate field:

$$\left(\frac{\phi^2}{\phi_0^2}\right)^{p_0} = \left(\frac{H}{H_0}\right)^{2M} \,. \tag{2.25}$$

A phantom EPN model implies condensation of the vector in a deceleration phase of expansion and 'evaporation' in a phase of acceleration, and vice versa for a quintessence EPN model. The phantom behavior could make one wary of the presence of instabilities. However, as shown in [44] and as reviewed below in 2.5, there exists a range of parameters in which linear perturbations are fully stable with no indications of strong coupling issues as far as we can identify within this effective theory.



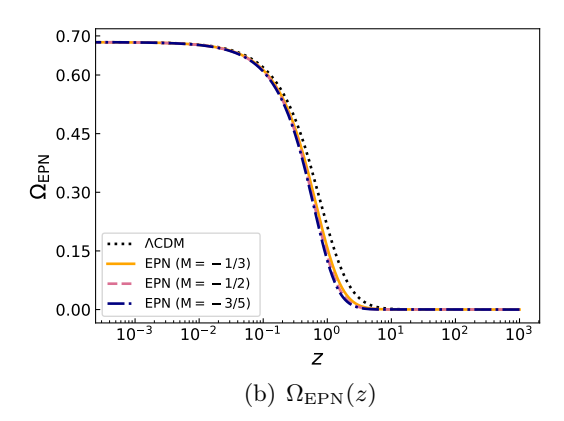


Figure 1. The evolution of the dark energy equation of state parameter $w_{\rm EPN}$ (left panel) and its energy fraction $\Omega_{\rm EPN}$ (right). The curves display the results in the $\Lambda{\rm CDM}$ model (dotted black), EPN special M model with M=-1/3 (solid yellow), and EPN general models with M=-1/2 (dashed pink) and M=-3/5 (dashed-dotted blue).

2.4 General EPN model

In the general EPN model, solving for the scalar component ϕ from (2.12) cannot be done in closed form for generic coefficient functions, or even for the generic parametrization of (2.15), cf. (2.17). However, particular choices of constants lead to simple closed-form models.

First, by setting $b_1 + e_1 = 0$, $b_3 + e_3 = 0$ and $b_2 + e_2 \neq 0$, the corresponding model

$$\rho_{\text{EPN}} = \frac{4 (c_m/3)^{3/2} \Lambda^4}{\sqrt{5(b_2 + e_2)}} \frac{\Lambda^2}{\sqrt{2} M_{\text{Pl}} H} = \rho_{\text{EPN0}} \left(\frac{H}{H_0}\right)^{-1}, \qquad (2.26)$$

permits an algebraic solution to the constraint equation, leading to an EPN energy density equivalent to that of the special M model with M = -1/2.

Second, with the choice $b_1 + e_1 = 0$, $b_2 + e_2 = 0$ and $b_3 + e_3 \neq 0$ one obtains

$$\rho_{\text{EPN}} = \frac{22 (c_m/7)^{7/5} \Lambda^4}{(b_3 + e_3)^{2/5}} \left(\frac{\Lambda^2}{2M_{\text{Pl}}H}\right)^{6/5} = \rho_{\text{EPN0}} \left(\frac{H}{H_0}\right)^{-6/5}, \tag{2.27}$$

likewise leads to an EPN energy density that mimics the special M model with M = -3/5. With this recurring theme, these models prompt us to hypothesize the existence of a family of non-minimally coupled models in EPN with an effective energy density and density fraction parameter that match the same Friedmann equation as in the special M model, Eq. (2.22).

In conclusion, cosmological background models obtained within the special M class discussed in Sec. 2.3 may also be derived as particular instances of the general, non-minimally coupled EPN model. The latter theories may be seen to be more natural from an EFT perspective, although it must be acknowledged that these models still require a tuning of coupling constants. On the other hand, it is worth pointing out that, although the modified Friedmann equations obtained via the two approaches are equivalent, the dynamics of perturbations will certainly differ. Let us also mention again that the one-parameter Friedmann equation thus obtained in EPN coincides also with the one obtained in GP theory, as well as in other very different set-ups such as braneworld models and theories of gravity which involve non-minimally coupled higher spin degrees of freedom (i.e. of spin > 0, including vector

fields). Any theory of modified gravity using a different derivation formalism or theories akin to f(T)/f(Q) can be recast as gravity with additional non trivial and non-minimally coupled degrees of freedom and can hence exhibit similar features. We note however that while expressing these theories as f(T)/f(Q) may be convenient to derive the classical background equations of motion, being able to identify the relevant degrees of freedom is essential not only to compare with observations but also to ascertain the stability and consistency of these models. Our analysis, which utilizes a broad and up-to-date catalog of datasets, is therefore applicable to all these models when restricted to the background evolution but goes beyond that.

2.5 Linear perturbations in the special EPN model

Given the aforementioned degeneracy of models at the background level, it is important to understand how perturbations affect the predictions of the theory. In the general EPN theory, the task is challenging due to the complexity of the equations, so for simplicity we consider here the special M model restricted to the case $p_0 = 1$. Our main aim here is to establish the stability criteria for perturbations, extending the analysis of [44] that focused on the case $p_1 = 2$.

Metric perturbations in the flat gauge are decomposed into two scalar modes α and χ , one transverse vector mode V_i and the transverse and traceless tensor mode h_{ij} ,

$$g_{\mu\nu}\mathrm{d}x^{\mu}\mathrm{d}x^{\nu} = -\left(1 + 2\frac{\alpha}{M_{\mathrm{Pl}}}\right)\mathrm{d}t^{2} + \frac{2}{M_{\mathrm{Pl}}}\left(\frac{\partial_{i}\chi}{M_{\mathrm{Pl}}} + aV_{i}\right)\mathrm{d}t\mathrm{d}x^{i} + a^{2}(t)\left(\delta_{ij} + \frac{h_{ij}}{M_{\mathrm{Pl}}}\right)\mathrm{d}x^{i}\mathrm{d}x^{j}.$$
(2.28)

The perturbed vector field is parametrized by two scalar perturbations $\delta \phi$ and χ_V along with a transverse vector mode Z_i ,

$$A^{0} = \phi(t) + \delta\phi, \quad A^{i} = \frac{1}{a^{2}} \delta^{ij} \left(aZ_{j} - \frac{a}{M_{\rm Pl}} \phi V_{j} + \frac{\partial_{j} \chi_{V}}{\Lambda} \right). \tag{2.29}$$

The spatial components of the four-velocity of a perfect fluid matter species can be split as

$$u_i = -\frac{\partial_i v}{M_{\rm Pl}^2} + \frac{U_i}{M_{\rm Pl}}, \qquad (2.30)$$

where v is a scalar and U_i is a transverse vector. Conservation of the energy-momentum tensor gives the continuity and Euler equations describing the time evolution of the i-th fluid density perturbation $\delta \rho_i$ and the matter momentum density $(\rho_i + P_i)v_i$,

$$M_{\rm Pl}^{2}\dot{\delta\rho_{i}} + 3M_{\rm Pl}^{2}H\left(1+c_{i}^{2}\right)\delta\rho_{i} + \frac{k^{2}}{a^{2}}\left(\rho_{i}+P_{i}\right)v_{i} + \frac{k^{2}}{a^{2}}\left(\rho_{i}+P_{i}\right)\chi = 0, \qquad (2.31)$$

$$(\rho_i + P_i)\dot{v}_i - 3Hc_i^2(\rho_i + P_i)v_i - M_{\rm Pl}^2c_i^2\delta\rho_i - M_{\rm Pl}(\rho_i + P_i)\alpha = 0, \qquad (2.32)$$

with δP_i representing the pressure perturbation and the fluid speed of sound is defined via $\delta P_i \equiv c_i^2 \delta \rho_i$. Combined with the EPN equations, it becomes evident that the EPN field influences the evolution of matter, affecting for instance matter aggregation and structure

formation. The resulting equations of motions for the scalar sector,⁴

$$(3H\hat{\omega}_{1} - 2\hat{\omega}_{4})\frac{\delta\phi}{\phi} - 2\hat{\omega}_{4}\frac{\alpha}{M_{\text{Pl}}} + \sum_{i}\delta\rho_{i} + \frac{k^{2}}{a^{2}\Lambda^{2}} \left[\hat{\mathcal{Y}} + \hat{\omega}_{1}\frac{\Lambda^{2}}{M_{\text{Pl}}^{2}}\chi - \hat{\omega}_{6}\Lambda\psi \right] = 0,$$

$$M_{\text{Pl}}^{2}\hat{\omega}_{2}\frac{\delta\phi}{\phi} + M_{\text{Pl}}\hat{\omega}_{1}\alpha + \sum_{i}(\rho_{i} + P_{i})v_{i} = 0,$$

$$(3H\hat{\omega}_{1} - 2\hat{\omega}_{4})\frac{\alpha}{M_{\text{Pl}}} - 2\hat{\omega}_{5}\frac{\delta\phi}{\phi} + \frac{k^{2}}{a^{2}\Lambda^{2}} \left[\frac{1}{2}\hat{\mathcal{Y}} + \hat{\omega}_{2}\frac{\Lambda^{2}}{M_{\text{Pl}}^{2}}\chi - \frac{\Lambda}{2}(\hat{\omega}_{2} + \hat{\omega}_{6}\phi)\frac{\psi}{\phi} \right] = 0,$$

$$\frac{\dot{\hat{\mathcal{Y}}}}{H} + \left(1 - \frac{\dot{\phi}}{H\phi}\right)\hat{\mathcal{Y}} + \frac{\Lambda^{2}}{H} \left[\hat{\omega}_{2}\frac{\delta\phi}{\phi} + 2\hat{\omega}_{7}\frac{\phi\psi}{\Lambda} + \hat{\omega}_{6}\left(2\frac{\alpha\phi}{M_{\text{Pl}}} + \delta\phi\right)\right] = 0,$$
(2.33)

with the definitions

$$\psi \equiv \chi_{V} + \frac{\Lambda}{M_{\rm Pl}^{2}} \phi \, \chi \,, \quad \hat{\mathcal{Y}} \equiv \Lambda^{2} \hat{\omega}_{3} \left(\frac{\delta \phi}{\phi} + 2 \frac{\alpha}{M_{\rm Pl}} + \frac{\dot{\psi}}{\Lambda \phi} \right) \,,$$

$$\hat{\omega}_{1} = \hat{\omega}_{2} - 2 M_{\rm Pl}^{2} H \,, \quad \hat{\omega}_{2} = -2 M_{\rm Pl}^{2} H \Omega_{\rm EPN} = \phi \, \hat{\omega}_{6} \,, \quad \hat{\omega}_{3} = -2 \phi^{2} \hat{q}_{V} \,,$$

$$\hat{\omega}_{4} = -3 M_{\rm Pl}^{2} H^{2} \left[1 - (2p_{1} - 3) \,\Omega_{\rm EPN} \right] \,, \quad \hat{\omega}_{5} = \frac{3}{2} \left(1 - 2p_{1} \right) H \hat{\omega}_{2} \,, \quad \hat{\omega}_{7} = \dot{\phi} \,\phi^{-3} \hat{\omega}_{2} \,,$$

$$\hat{q}_{V} = 1 - \left(2 + \frac{\dot{\phi} + H \phi}{\Lambda^{2}} \right)^{-1} \left[\alpha_{1} - 2 \left(1 - 2 \frac{H \phi}{\Lambda^{2}} \right) \alpha_{2,X} + \frac{H \phi}{\Lambda^{2}} \left(2 - \frac{H \phi}{\Lambda^{2}} \right) \alpha_{3,X} \right] \,, \quad (2.34)$$

determine the two metric perturbations α and χ , the constraint on $\delta\phi$, and the evolution of the matter perturbation and ψ , which are dynamical degrees of freedom.

The absence of ghost, gradient and tachyon instabilities for the EPN and matter perturbations near the de Sitter fixed point ($\Omega_{\rm EPN} \to 1$) translate into the conditions of positivity of the following quantities [44]:

$$\hat{q}_V = 1 - \frac{b_1 \tilde{c}_m^{-p_1/2} + (10b_2 + 8b_3)\tilde{c}_m^{-1} + (c_1 + 10c_2 + 8c_3)\tilde{c}_m^{-1/2}}{(1 + p_1^{-1}/2)(1 - \Omega_{\text{EPN}})},$$
(2.35)

$$\hat{c}_V^2 \hat{q}_V = 1 - \frac{1}{2} b_1 \tilde{c}_m^{-p_1/2} - (3b_2 + b_3) \tilde{c}_m^{-1} - \left(\frac{c_1}{2} + 3c_2 + c_3\right) \tilde{c}_m^{-1/2}, \tag{2.36}$$

$$\hat{m}_V^2 H^{-2} = 5, (2.37)$$

$$\hat{q}_{S,\psi} = \frac{3\Lambda^2}{M_{\rm Pl}^2} \frac{(\Omega_{\rm EPN} - M^{-1})\tilde{c}_m}{(1 - \Omega_{\rm EPN})^2} \,, \tag{2.38}$$

$$\hat{c}_{S,\psi}^2 = \frac{\tilde{c}_m^{1/2}}{6p_1\hat{q}_V},\tag{2.39}$$

$$\hat{m}_{S,\psi}^2 H^{-2} = \frac{45}{4} - \frac{6(1+p_1^{-1})^2 \tilde{c}_m^{1/2}}{\hat{q}_V (1-\Omega_{\text{EPN}})} - \frac{\tilde{c}_m}{\hat{q}_V^2 (1-\Omega_{\text{EPN}})^2}, \qquad (2.40)$$

$$\hat{m}_{S,M}^2 H^{-2} = \frac{3\tilde{c}_m^{1/2}}{2\hat{q}_V (1 - \Omega_{EPN})},$$
(2.41)

⁴We refer the reader to [44] for details on the calculations that follow. We also ignore from now on vector and tensor perturbations. In the special model that we focus on in our perturbation analysis, tensor modes evolve exactly as in GR and therefore do not give any additional constraints. Moreover, matter (assuming a perfect fluid) and metric vector modes are decoupled from those of the EPN field, so the vector sector also does not affect the confrontation of the model with data.

where $\tilde{c}_m \equiv c_m/6$. Here the \hat{q} parameters represent the coefficients of the kinetic terms of the perturbations, the \hat{c}_S represent the respective speed of sounds, and the \hat{m}_S represent the effective masses; in particular, $\hat{m}_{S,\mathrm{M}}$ is the effective mass of the matter perturbation in the scalar sector, assumed here to be given by a single perfect fluid (a good approximation during the matter- and dark energy-domination eras, including the transition between the two). We also emphasize that these results are valid up to order $(1 - \Omega_{\mathrm{EPN}})^0$ in an expansion around the fixed point.

Stability under ghost-, gradient- and tachyon-type solutions demands the positivity of all these quantities. Actually, $\hat{m}_{S,\psi}^2$ has a negative-definite contribution at order $(1-\Omega_{\rm EPN})^{-1}$, which we omitted as it can be canceled by setting

$$b_1 + e_1 = p_1^{-1} \tilde{c}_m^{(3-M^{-1})/4}, (2.42)$$

which has already been imposed in Eq. (2.40).

A simple and convenient choice that meets the stability criteria under ghosts and gradients is

$$b_1 = c_1 = b_2 = c_2 = b_3 = c_3 = -1,$$
 (2.43)

which we will adopt in the numerical analysis that follows. Taking into account Eq. (2.19), this leaves us with two free parameters: the coefficient M of the Friedmann equation and the mass m of the Proca field (equivalently, the constants p_1 and c_m). This set-up differs significantly from the GP model studied in [41], in which set-up $\hat{m}_{S,\psi}^2 H^{-2} \sim -2|e_1|\tilde{c}_m^{-1/2} (1-\Omega_{\rm EPN})^{-2}$ is negative definite. We also remark that the quintessence-like model (M>0) develops a ghost instability as $\hat{q}_{S,\psi}$ diverges toward $-\infty$ according to Eq. (2.38). Coincidentally, it is also observationally disfavored at the background level, as discussed in Sec. 4.

As c_m (and b_i , c_i) only appears in $\hat{\omega}_3$ in the master equations of the scalar perturbation, Eqs. (2.33), we see that we can achieve the effective decoupling of the EPN scalar mode from ordinary matter in the limit $\hat{\omega}_3 \propto \hat{q}_V \to 0$. If $b_i, c_i = \mathcal{O}(1)$, this in turn implies $c_m \propto m^2 \to \infty$ (remembering that we set $p_0 = 1$), i.e. a very heavy field, making it reasonable that perturbations should be suppressed in this limit. We will verify this explicitly in our analysis. Related to this, we also point out that c_m is introduced in the first place precisely because one expects it to be $\mathcal{O}(1)$ in a consistent EFT, where one has $\Lambda \sim (mM_{\rm Pl})^{1/2}$. We will further comment on this point in Sec. 5.

3 Data and analysis methodology

In this section, we introduce the analysis methodology and the astrophysical and cosmological datasets to investigate the EPN models described in Section 2. We focus on two particular realizations of the EPN model. First, we consider the special M model with M ranging from -1/2 (phantom) to 1/2 (quintessence), while ignoring the effect of perturbations of the dark energy fluid entirely. Formally, this amounts to setting $\hat{\omega}_2 = \hat{\omega}_3 = \hat{\omega}_6 = 0$, $\hat{\omega}_4 = -3M_{\rm Pl}^2H^2$ and $\hat{\omega}_1 = -2M_{\rm Pl}^2H$ in Eqs. (2.33), resulting in the decoupling of the EPN perturbations from the matter and metric ones, thus reducing the perturbation equations back to the Λ CDM set-up, with the background evolution substituted by Eq. (2.22). One expects this decoupled theory to be a suitable approximation for describing most high-redshift observations, since $|\hat{\omega}_2| \ll M_{\rm Pl}^2H$ (cf. (2.34)) during the matter-dominated era when the large-scale structure formed. By the same token, we expect this description to break down at low redshifts, and indeed we will see that perturbations do have an important effect on the structure growth

rate. We also do not expect this approximation to be valid for the quintessence-like models (0 < M < 1/2), since we have seen that perturbations are unstable near the de Sitter fixed point in this set-up. Nevertheless, we still include this parameter range in our analysis, for the sake of completeness on the one hand, but also because of the potential applicability to other theories.

In the second realization we extend the analysis to take full account of perturbations, focusing on their effect on observables such as the matter power spectrum and the growth history. Let us clarify the terminology we employ for the different model realizations:

- EPN special M model: This refers to the realization mentioned above in which we ignore the EPN perturbation, either fixing M or allowing it to vary in the prior range [-0.5, 0.5];
- EPN very special model: This is the model discussed in Sec. 2.3, i.e. the EFT-motivated member of the special EPN class with M = -1/3, taking into account all scalar perturbations;
- EPN full special model: This is the special EPN model, taking all scalar perturbations into account, and without fixing M. We let the latter vary in the prior range $[-1/2, -10^{-8}]$ (recall that EPN perturbations are stable only for M < 0).⁵

Furthermore, for the latter two cases we choose the prior range [-1,6] for $\log_{10} c_m$. As discussed in the previous section, sampling over parametrically large values of c_m will allow us to explore the decoupling regime of EPN perturbations

We evaluate the models with the Boltzmann code CAMB [91, 92]. For the Λ CDM model, the standard six-parameter basis is used: the physical densities of baryons $\Omega_{\rm b0}h^2$ and cold dark matter $\Omega_{\rm c0}h^2$, the approximated acoustic angular scale $\theta_{\rm MC}$, the optical depth $\tau_{\rm reio}$, the amplitude of primordial scalar perturbations $\ln(10^{10}A_{\rm s})$, and the scalar spectral index $n_{\rm s}$. The full special EPN model is implemented in CAMB with the additional parameters M and c_m . In view of the modifications to the matter perturbation evolution, we have preliminarily considered both the analytic halofit [93, 94] and iterative HMcode [95] halo models for the nonlinear matter power spectrum. Having checked that both produce identical results given randomly drawn parameters (and provided HMcode converges, as indeed it does except for rare edge cases), we have picked HMcode as our halo model.

A summary of cosmological parameters and their priors for different models are provided in Table 1. We assume the BBN prior on the baryon density $\Omega_{\rm b0}h^2$ and a cut $50 < H_0 < 100$ on the Hubble constant H_0 , translated here to $\theta_{\rm MC}$ [96]. Following standard practice, the prior distributions for the latter as well as for all remaining parameters are chosen as flat. Additionally, we consider a single massive neutrino and two massless neutrinos in the

$$\begin{split} \frac{\alpha}{M_{\rm Pl}} &= \frac{H\partial_t {\rm etak} - {\rm etak} \dot{H}}{kH^2} \;, \quad \frac{\sum_i \delta \rho_i}{M_{\rm Pl}^2} = \frac{{\rm dgrho_{noDE}}}{a^2} - 3 \frac{\rho_{\rm M}}{M_{\rm Pl}^2} (1+w_{\rm M}) \frac{{\rm etak}}{k} \;, \\ \frac{\chi}{M_{\rm Pl}^2} &= a \frac{z}{k} - \frac{{\rm etak}}{kH} + \frac{3a^2 \partial_t {\rm etak}}{k^3} \;, \quad \frac{\sum_i (\rho_i + P_i) v_i}{M_{\rm Pl}^4} = \frac{{\rm dgq_{noDE}}}{ak} + \frac{\rho_{\rm M} (1+w_{\rm M})}{M_{\rm Pl}^2 H} \frac{{\rm etak}}{k} \;. \end{split}$$

⁵The case M=0 yields ill-defined perturbations equations, which is why we exclude this value from our prior. The reason can be traced back to the definition of M in terms p_0 and p_1 , Eq. (2.20): having fixed $p_0=1$, M must be strictly non-zero.

⁶The scalar perturbation equations, Eqs. (2.33), are transported to CAMB variables via the following mapping:

Paramet		Prior		
	$\Omega_{ m b0}h^2$	norm	0.0222	0.0005
	$\Omega_{\mathrm{c}0}h^2$	flat	0.001	0.99
$\Lambda { m CDM}$	$100 heta_{ m MC}$	flat	0.5	10
ACDM	$\ln(10^{10}A_{\rm s})$	flat	1.61	3.91
	$n_{ m s}$	flat	0.8	1.2
	$ au_{ m reio}$	flat	0.01	0.8
EPN special M	M	flat	-0.5	0.5
EPN full special	M	flat	-0.5	-10^{-8}
Er iv run special	$\log_{10} c_m$	flat	-1	6

Table 1. The model parameters of Λ CDM and EPN considered in this work. We consider normal and flat prior distributions, indicated in the third column. In the former case, the fourth and fifth columns denote respectively the mean and width; in the latter case, they denote respectively the minimum and maximum.

calculations, fixing the sum of neutrino masses as $\sum m_{\nu} = 0.06$ eV. The total matter density parameter at $\Omega_{\rm m0}$ thus includes the contributions of cold dark matter, baryons, and one neutrino species.

We make use of the Cobaya [97–100] Markov Chain Monte Carlo (MCMC) sampler to generate the posterior distribution of the full set of cosmological parameters. For each dataset, two chains are deployed based on the early convergence test, and we consider the chains as converged when the stopping criteria of intra-chain and inter-chain R-1 < 0.01 are satisfied. We use GetDist [101] to perform statistical analyses of MCMC samples and to plot the posteriors.

The list of observational datasets and likelihoods used in this work is:

- Cosmic Microwave Background (CMB) temperature and polarization anisotropy measurements from the Planck satellite. This rich and well-analyzed dataset is the main basis of our analysis. The CMB dataset used in this work includes: (i) Planck 2018 low multipole ($2 \le \ell \le 30$) temperature anisotropy power spectrum C_{ℓ}^{TT} , reconstructed using the Commander likelihood; (ii) Planck 2018 low multipole ($2 \le \ell \le 30$) large-scale E-mode polarization power spectrum C_{ℓ}^{EE} , derived from the Simall likelihood; (iii) high multipole power spectra of temperature and polarization anisotropies, C_{ℓ}^{TT} , C_{ℓ}^{TE} , C_{ℓ}^{EE} , derived from the NPIPE PR4 Planck CamSpec likelihood [1]; (iv) lensing potential power spectrum, derived from NPIPE PR4 lensing reconstruction data [4, 65]. We denote the combination of these likelihoods as "CMB".
- The Dark Energy Spectroscopic Instrument (DESI) has measured the baryon acoustic oscillation (BAO) signal from galaxy clustering correlations using tracers from galaxies, quasars and the Ly α forest in the redshift range $0.1 \le z \le 4.2$. We utilize 12 BAO measurements from the DESI Data Release 1 [15, 66, 67], which we denote here as "DESI".

The parameter $R = \max_{\theta} \sqrt{1 + \operatorname{var}_i(\operatorname{mean}_{\operatorname{seg}_i}(\theta))/\operatorname{mean}_i(\operatorname{var}_{\operatorname{seg}_i}(\theta))}$ probes the consistency of parameter distributions $P(\theta)$ across chains for inter-chain R or segments within a particular chain for intra-chain R.

⁸The use of the CMB dataset sets our work apart from [57, 58]. A comparison with these references would require the exclusion of the CMB dataset.

- The PantheonPlusSH0ES supernova catalog, containing the PantheonPlus sample [68] (comprising 1701 light curves measured from 1550 Type Ia supernovae over the redshift range 0.001 < z < 2.26), removing the data points in the redshift range z < 0.01, with anchoring of SNIa standardized absolute magnitudes with SH0ES [2]. We will refer to the combination of these supernova data as "PPS".
- Galaxy Survey: We also consider BAO, growth rate and σ₈ measurements by the 6-degree Field (6dF) Galaxy Survey [70, 71] and the Sloan Digital Sky Survey (SDSS) Data Release 16 [69], collectively referred to as "SDSS" here. This dataset is mutually exclusive of DESI BAO dataset.⁹

We also present two supplementary datasets in some of our plots that are excluded from the cosmological fit. These include an additional $f\sigma_8$ dataset (table 2 of [102], with data entries from [71, 103–114]), SDSS DR7 LRG dataset [115] and eBOSS DR14 Ly- α dataset [116] (presented in Fig. 7), and the weak lensing dataset from the Dark Energy Survey (DES) Y3 data release (presented in Fig. 4).

Information Criteria IC & Bayesian Evidence: To compare between different datasets and models, we primarily utilize 6 probes of Information Criteria (IC), defined in Appendix B. The traditional Bayesian evidence B, the Deviance Information Criteria (DIC) and the Widely Applicable Information Criteria (WAIC) [117] are for model comparison, while the Bayesian ratio R, the goodness of fit, and the suspiciousness [118–120] are employed for data tension detection. While probes such as DIC, WAIC and Bayesian ratio can be easily interpreted using the Jeffreys' scale (see Table 5), the Goodness-of-Fit and Suspiciousness require further processing. As these two probes follow the BMD-dimensional χ distribution [120], we may convert them into the usual confidence level σ value as CDF_1^{-1} ($\mathrm{CDF}_{\mathrm{BMD}}$ ($\sqrt{\mathrm{BMD}} + 2z$)), where CDF_d is the cumulative distribution function of a d-dimensional χ distribution and z stands for either the Goodness-of-Fit or Suspiciousness; see Appendix B for the definitions.

4 Results

This Section presents the results of our analysis. In Sec. 4.1 we present cosmological constraints on the parameters H_0 , $\Omega_{\rm m0}$, S_8 and M obtained from the $\Lambda{\rm CDM}$ and EPN models at the background-modified level. In Sec. 4.2 we compare the matter power spectrum and growth rate obtained in $\Lambda{\rm CDM}$ and EPN special model with and without perturbations, paying particular attention to the effects of the mass parameter c_m . In Sec. 4.3 we evaluate and compare the performance of all models according to the IC described in Sec. 3 and in Appendix B, discussing in particular the discrepancy between early- and late-time universe fits through the CMB TT power spectra and distance modulus reconstructed from the MCMC chains.

4.1 Parameter constraints

Table 2 summarizes the parameter constraints obtained from the data fits of Λ CDM, two EPN models with fixed M (the special M model with M = -1/3 and the model M = -1/2 motivated by the considerations of Sec. 2.4) as well as the case with free M. Recall that we

⁹Due to overlapping regions of observation between SDSS and DESI, the DESI group has cautioned against naïve combinations of the two datasets [15]. For this reason, we only consider SDSS and DESI data individually in our analysis.

Model/Parameters	CMB	CMB + DESI	CMB + DESI + PPS	DESI	PPS
ΛCDM					
$H_0 \ [\text{km s}^{-1} \ \text{Mpc}^{-1}]$	67.21 ± 0.46	67.86 ± 0.37	68.40 ± 0.34	68.70 ± 0.79	73.6 ± 1.0
$\Omega_{ m m0}$	0.3158 ± 0.0064	0.3067 ± 0.0049	0.2999 ± 0.0044	0.295 ± 0.015	0.332 ± 0.018
σ_8	0.8078 ± 0.0054	0.8066 ± 0.0056	0.8060 ± 0.0059		
$\overset{\circ}{S_8}$	0.829 ± 0.011	0.8156 ± 0.0091	0.8058 ± 0.0088		
EPN $M = -1/3$					
$H_0 [\mathrm{km \ s^{-1} \ Mpc^{-1}}]$	71.91 ± 0.50	71.66 ± 0.39	71.52 ± 0.36	72.36 ± 0.89	73.6 ± 1.0
$\Omega_{ m m0}$	0.2753 ± 0.0057	0.2780 ± 0.0043	0.2798 ± 0.0041	$0.298^{+0.013}_{-0.015}$	0.378 ± 0.019
σ_8	0.8344 ± 0.0055	0.8281 ± 0.0056	0.8286 ± 0.0055	-0.013	
S_8	0.799 ± 0.011	0.7971 ± 0.008	0.8001 ± 0.0083		
EPN $M = -1/2$					
$H_0 [{\rm km \ s^{-1} \ Mpc^{-1}}]$	73.54 ± 0.53	73.11 ± 0.39	72.68 ± 0.37	73.84 ± 0.87	73.7 ± 1.0
$\Omega_{ m m0}$	0.2635 ± 0.0056	0.2681 ± 0.0041	0.2728 ± 0.0040	0.298 ± 0.014	0.397 ± 0.019
σ_8	0.8352 ± 0.0056	0.8361 ± 0.0056	0.8367 ± 0.0057		
S_8	0.783 ± 0.011	0.7905 ± 0.0088	0.7979 ± 0.0084		
EPN special M					
$H_0 [{\rm km \ s^{-1} \ Mpc^{-1}}]$	$65.3^{+5.1}_{-4.3}$	69.9 ± 1.2	69.82 ± 0.63	$68.9^{+3.7}_{-2.4}$	73.5 ± 1.0
$\Omega_{ m m0}$	$0.340^{+0.034}$	0.2912 ± 0.0098	0.2905 ± 0.0054	0.294 ± 0.016	$0.315^{+0.058}_{-0.051}$
σ_8	0.75 ± 0.17	0.8180 ± 0.0086	0.8164 ± 0.0067		
S_8	$0.75_{-0.35}^{+0.035} \\ 0.846_{-0.044}^{+0.034}$	0.806 ± 0.011	0.8033 ± 0.0087		
M	$0.12^{+0.32}_{-0.15}$	$-0.164^{+0.11}_{-0.091}$	$-0.136^{+0.057}_{-0.051}$	-0.05 ± 0.23	> -0.0924

Table 2. Cosmological parameter constraints from different data combinations and priors, in the Λ CDM and three EPN special M models ($M=-1/3,\ M=-1/2,\$ and M as fitting parameter). Results are quoted for the marginalized means and 68% confidence intervals or lower limit.

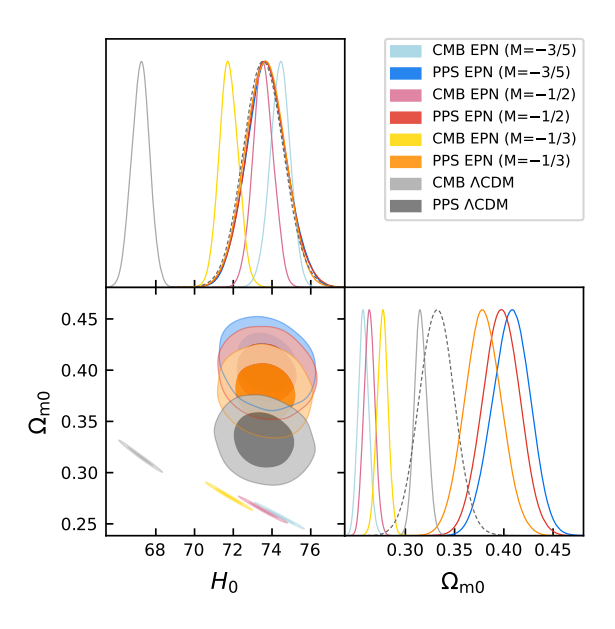


Figure 2. Marginalized posterior constraints on H_0 and $\Omega_{\rm m0}$ using CMB and PPS data in Λ CDM and three EPN special M models. Contours indicate 68% and 95% confidence level intervals.

begin by focusing on the background-modified level, i.e. ignoring perturbations of the EPN field, but including metric and matter perturbations; see Sec. 3 for details on our set-up.

Remarkably, we see that the result for H_0 in the EPN special M model with M=-1/3

Model/Parameters	CMB	CMB + SDSS
ACDM	CIVID	
$H_0 \ [\text{km s}^{-1} \ \text{Mpc}^{-1}]$	67.21 ± 0.46	67.56 ± 0.36
$\Omega_{\rm m0}$	0.3157 ± 0.0065	0.3109 ± 0.0049
σ_8	0.8075 ± 0.0056	0.8084 ± 0.0054
S_8	0.828 ± 0.011	0.8229 ± 0.0091
DIC	5498.05 ± 0.10	5510.10 ± 0.40
WAIC	5498.95 ± 0.07	5511.04 ± 0.24
$-\ln B$	5498.59 ± 0.27	5510.90 ± 1.12
EPN $M = -1/3$		
$H_0 \ [{\rm km \ s^{-1} \ Mpc^{-1}}]$	71.91 ± 0.50	71.21 ± 0.40
$\Omega_{ m m0}$	0.2753 ± 0.0057	0.2832 ± 0.0046
σ_8	0.8344 ± 0.0055	0.8348 ± 0.0058
S_8	0.799 ± 0.011	0.8112 ± 0.0095
$\Delta { m DIC}$	0.42 ± 0.15	4.31 ± 0.37
$\Delta \mathrm{WAIC}$	1.09 ± 0.77	4.78 ± 0.37
$\Delta - \ln B$	-0.66 ± 2.69	5.03 ± 0.58
EPN very special		
$H_0 \ [{\rm km \ s^{-1} \ Mpc^{-1}}]$	72.21 ± 0.56	71.29 ± 0.41
$\Omega_{\mathrm{m}0}$	0.2719 ± 0.0061	0.2824 ± 0.0047
σ_8	0.8499 ± 0.0059	0.8494 ± 0.0060
S_8	0.809 ± 0.011	0.8241 ± 0.0091
$\log_{10} c_m$	$4.42^{+0.66}_{-1.1}$	$4.83^{+1.1}_{-0.49}$
$\Delta { m DIC}$	-0.15 ± 0.26	5.28 ± 0.48
$\Delta \mathrm{WAIC}$	0.13 ± 0.91	5.31 ± 0.24
$\Delta - \ln B$	-0.31 ± 2.02	4.19 ± 1.10
EPN full special		
$H_0 \ [{\rm km \ s^{-1} \ Mpc^{-1}}]$	71.41 ± 0.81	$70.16^{+0.46}_{-0.56}$
$\Omega_{ m m0}$	0.2777 ± 0.0075	0.2898 ± 0.0053
σ_8	0.8424 ± 0.0082	0.8365 ± 0.0071
S_8	0.810 ± 0.011	0.8221 ± 0.0092
M	$-0.260^{+0.051}_{-0.076}$	$-0.202^{+0.046}_{-0.024}$
$\log_{10} c_m$	$4.65^{+1.0}_{-0.77}$	> 5.08
$\Delta \mathrm{DIC}$	-0.40 ± 0.20	2.22 ± 0.41
Δ WAIC	-0.23 ± 0.14	2.95 ± 0.27
$\Delta - \ln B$	-0.72 ± 2.32	2.54 ± 1.41

Table 3. Cosmological parameter constraints from different data combination and priors, in the Λ CDM, the special M with M=-1/3 (without dark energy perturbations), the very special and the full special models. Results are quoted for the marginalized means and 68% confidence intervals or lower limit.

is 71.91 ± 0.50 km s⁻¹ Mpc⁻¹ when derived from CMB data and 73.6 ± 1.0 km s⁻¹ Mpc⁻¹ from supernova PPS data. The Hubble tension in this set-up is therefore significantly reduced down to $\sim 1.52\sigma$ (in comparison with $\sim 5.81\sigma$ in Λ CDM). Furthermore, when leaving M as a fitting parameter, we find that the more negative M is, the higher H_0 derived from the CMB dataset becomes, until it matches the local H_0 value of PPS at $M \simeq -1/2$ (cf. Table 1).

On the other hand, along with the decrease in the Hubble tension, a tension in the measurement of $\Omega_{\rm m0}$ from CMB and PPS datasets arises; see Fig. 2. This behavior is consistent with other phantom-like models (see e.g. [37, 121]). This effect may be understood as follows. Although phantom dark energy stretches the distance to the last scattering surface, thus leading to a greater H_0 as predicted by CMB data in order to match the acoustic peak scale, it also dims type-Ia supernovae more than Λ CDM does. The only way to compensate for this dimming, given the local H_0 measurements of SH0ES, is to increase $\Omega_{\rm m0}$, which in

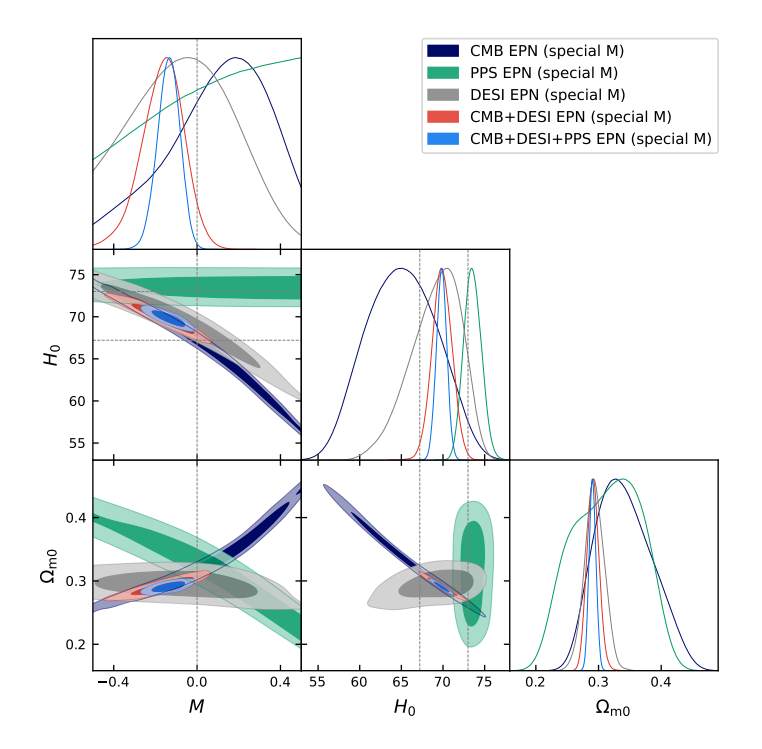


Figure 3. Marginalized posterior constraints on M, H_0 and $\Omega_{\rm m0}$ using different (combinations of) datasets in the EPN special M model. Contours indicate 68% and 95% confidence level intervals. Dashed lines indicate best fit values for $\Lambda{\rm CDM}$, i.e. with M=0. Although the CMB, DESI and PPS datasets do not individually constrain the parameter M well, the combined dataset CMB + DESI + PPS favors M<0 at the $\gtrsim 2\sigma$ confidence level ($\gtrsim 1\sigma$ for CMB + DESI).

turn reduces the amount of dark energy. This is reflected by the comparatively large $\Omega_{\rm m0}$ deduced in EPN from the PPS dataset; cf. Table 2.

We also discover that the result for S_8 in the very special EPN model inferred from the CMB dataset is in mild tension with that deduced from the SDSS dataset, as shown in Table 3. This tension is even more evident in Fig. 6, which shows that EPN models consistently predict stronger matter perturbation spectra compared with Λ CDM at and below the BAO acoustic scale. However, this is not necessarily a drawback considering the derived value $S_8 = 0.776 \pm 0.017$ for Λ CDM from DES Y3 [118], as is manifest in Fig. 4(a). This behavior is again not specific to EPN, as the same behavior happens for the CPL phenomenological model with a matching cosmographic equation of state [121]. Quantifying more precisely by how much EPN performs better with the DES weak lensing dataset is left to further studies as including these data within our current MCMC analysis proves to be computationally demanding and beyond the direct remit of this work. 11

 $^{^{10}}$ As each dataset measures matter spectrum power at a different redshift, Fig. 6 pulls all data to the present day via the transfer function. This makes the data points model-dependent. Despite this caveat, we can still conclude that EPN models do introduce tension between CMB and SDSS, given that the models swing from weakly favored over Λ CDM for the CMB dataset to moderately disfavored for the CMB + SDSS dataset, as shown in Table 3.

¹¹The S_8 probe, designed to eliminate the misalignment between $f\sigma_8$ and σ_8 via the theoretically motivated formula $f \sim \Omega_{\rm M}^{0.55}$, no longer describe the matter perturbation history correctly in EPN models, as shown in Fig. 7. It is therefore difficult to interpret the S_8 values presented in Table 3, in particular when compared with the derived value of S_8 from the DES dataset. However, we do treat SDSS data as likelihoods over $f\sigma_8$.

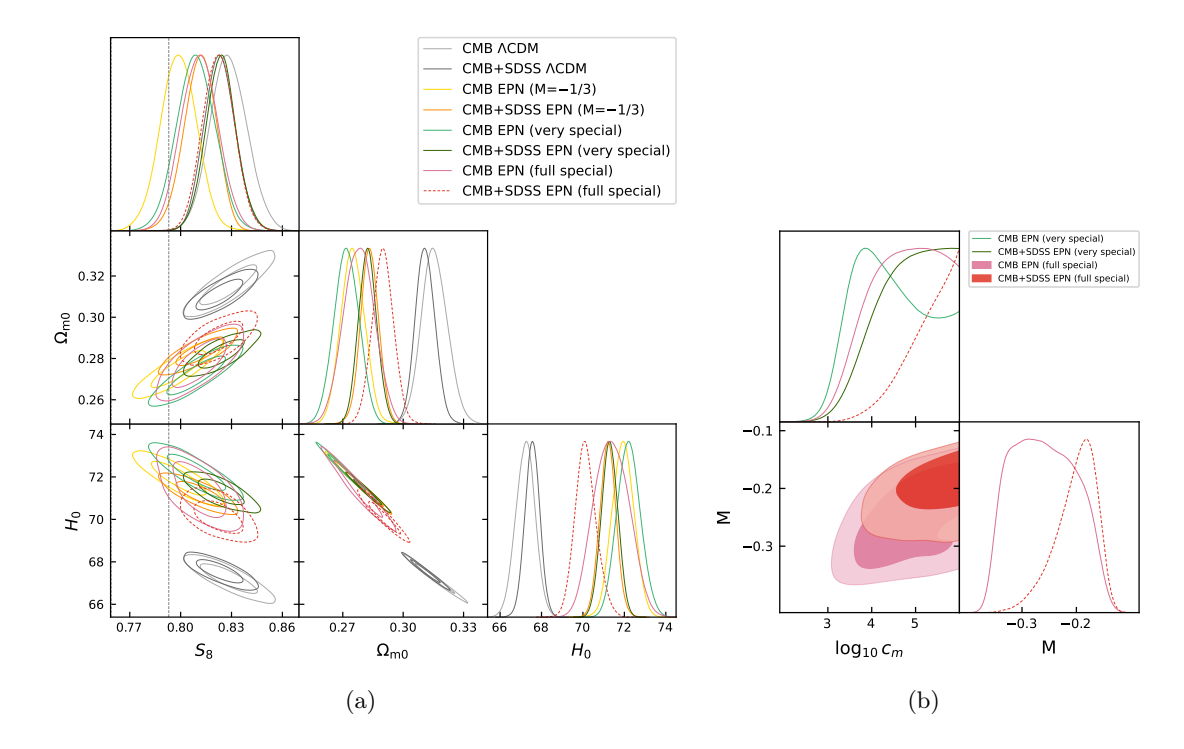


Figure 4. Left panel: 68% and 95% marginalized posterior constraints on S_8 , $\Omega_{\rm m0}$ and H_0 using CMB, CMB+SDSS datasets in Λ CDM, the EPN special M (M=-1/3), very special and full special models. The vertical dashed line in S_8 corresponds to the best fit + 1 σ value $S_8=0.776\pm0.017$ derived for Λ CDM from DES Y3. Right panel: marginalized posterior constraints on M and the Proca mass parameter c_m in the EPN very special and full special models from the same two datasets.

More interestingly, when allowing for a variable EPN parameter M in the analysis, the CMB + DESI + PPS combination constrains M to $-0.136^{+0.057}_{-0.051}$, i.e. a clear departure from Λ CDM (M=0) at the $\gtrsim 2\sigma$ level, while for the CMB + DESI combination the result is $M=-0.164^{+0.11}_{-0.091}$, which is less tight but still $\gtrsim 1\sigma$. Fig. 3 displays the constraints on M, H_0 and $\Omega_{\rm m0}$ and their posterior distributions. See also Fig. 12 in Appendix C for the complete constraint plot of cosmological parameters from the CMB + DESI + PPS dataset.

4.2 Matter power spectrum and structure growth

Next we investigate the impact of perturbations in the data fits, considering the model realizations given by the EPN very special and full special models, cf. Sec. 2.5. We focus in particular on the analysis of the structure growth history as inferred from the CMB and SDSS datasets.

Fig. 4 shows the fitting contours obtained from different combinations of datasets as well as the constraints on the Proca mass parameter c_m . A parametrically large¹³ value

All the tension probes and IC values presented in Table 3 thus correctly evaluate the SDSS dataset, including the comparison between different models.

¹²This is a looser constraint than the one obtained in [41] in the context of GP theory; the reason is likely due to the omission in that reference of SNIa anchoring, which is known to be detrimental to phantom-like models, cf. Fig. 10(d). Note incidentally that the parameter s in [41] is equivalent to -M here.

 $^{^{13}}$ By parametrically large, we mean a mass m two or three orders of magnitude larger than the scale of dark energy, which is hence still well within the acceptable range. Given that the initial prior is flat and enables the code to explore much larger value of the mass, it is very encouraging to note that the favored value converges

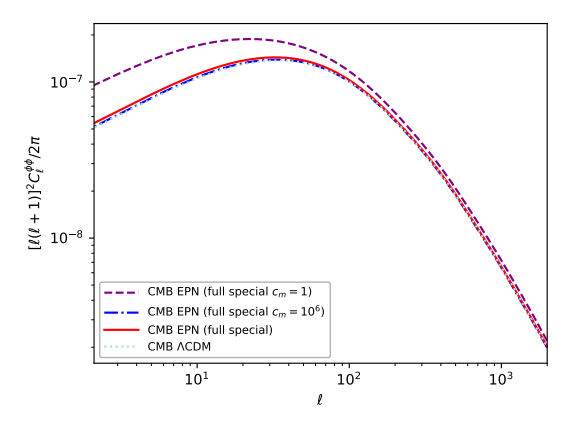


Figure 5. The lensing potential of the best-fit Λ CDM model and the EPN full special model given the best-fit parameters for the CMB dataset, with different values of the Proca mass parameter c_m , including the best-fit value $c_m = 10^{4.48}$ (red curve). The strong enhancement for $c_m = \mathcal{O}(1)$ values is manifest.

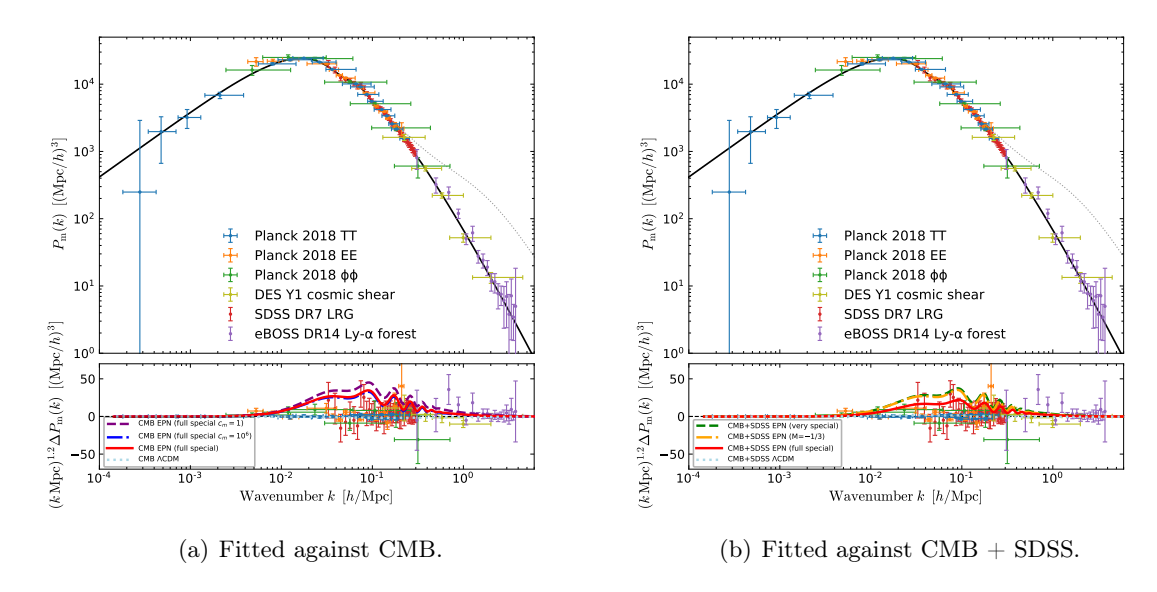


Figure 6. Best-fit matter power spectrum (top panels) and the residue (bottom) against the best-fit ΛCDM spectrum. In the top panels (which are identical) solid curves represent the linear power spectrum while dotted curves represent the non-linear power spectrum (data taken from [122]). Bottom-left: Residue plot for the EPN full special model from the CMB dataset, for fixed and varying c_m values (same color-coding as Fig. 5). Bottom-right: Residue plot for the EPN very special, full special, and the background only M = -1/3 models, fitted against the CMB+SDSS dataset. There is an evident discrepancy between ΛCDM and the EPN models, in particular at and below the BAO scale, with the EPN special background-only model slightly closer to ΛCDM than the very special model. There is a modest power suppression upon including SDSS data.

of c_m is strongly preferred for both EPN model realizations. As demonstrated by Fig. 5, such a preference is induced by the foreground effect of the CMB, in particular the late-

towards values of the mass which are within the theoretically reasonable range.

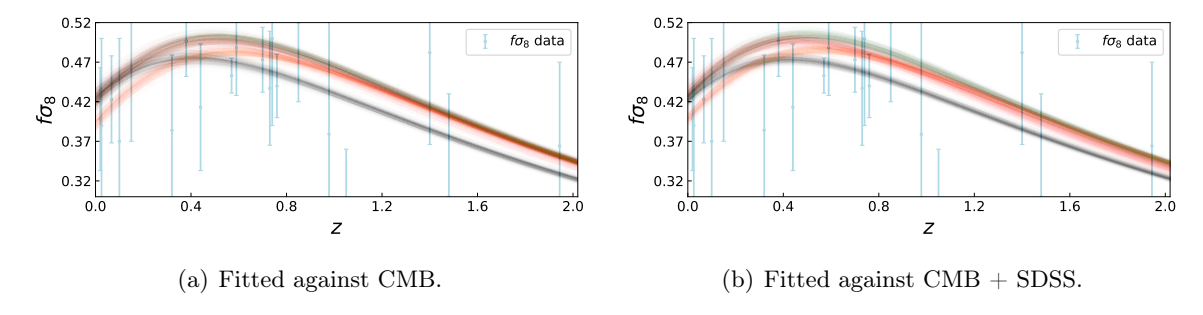


Figure 7. Structure growth rate $f\sigma_8$ as a function of redshift z. Curves show the fits against CMB (left panel) and against CMB+SDSS (right) datasets in Λ CDM (black), EPN special M model with M = -1/3 (yellow), EPN very special model (green) and EPN full special model (red). Data points were taken from Table 2 of [102].

time integrated Sachs-Wolfe and the lensing effects as well as the matter perturbation growth history, since the EPN model introduces an enhancement of the effective Newton constant, $G_{\rm eff}$, altering the low- ℓ CMB spectrum and $f\sigma_8$;¹⁴ see Appendix A for details. The excess spectrum power is due to the EPN scalar contribution to the scalar potential, which can be suppressed by taking the decoupling limit, hence the preference for parametrically large values of c_m corresponding to $m \sim \mathcal{O}\left(10^2 H_0\right)$, where H_0 is the Hubble parameter today, so this is still within the acceptable range for the mass. It is also worth commenting on the upper confidence intervals on c_m quoted in Table 3. In view of the irregular posterior distributions, cf. Fig. 4(b), this should not be seen as an upper bound but rather as indicating that excessively large mass values are less preferred. This is likely to compensate for the excessive 'phantomness' of the EPN field at the background level. The results of our analysis therefore do not confirm the claim made in [39] on the existence of an upper bound on the mass of the Proca field from cosmological observations. Rather our analysis indicate no clear sign of an upper bound.

The $f\sigma_8$ measurements from Λ CDM and the EPN special model with and without dark energy perturbations are presented in Fig. 7. The tendency of a greater $f\sigma_8$ before the dark energy-dark matter transition, and a lower value afterwards, is consistent with the background evolution history, i.e. a phantom-like dark energy fluid leading to a greater $\Omega_{\rm M}$ before the transition and a lower $\Omega_{\rm M}$ afterwards.

One might naively have expected a sizable alteration of the growth rate at low redshifts from the modification of the matter perturbation equations by the EPN terms, cf. Eqs. (2.34). However, a careful derivation shows that these modifications are actually $\mathcal{O}(\Omega_{\text{EPN}}^2)$, implying a significant effect on the growth history only at very low redshifts and therefore essentially unconstrained by current observations. Curiously, the modification brings the $f\sigma_8$ value back to that of Λ CDM at around the present time, regardless of the value of the background parameter M. Whether this is a mere coincidence or a signal of hidden structures within EPN theory remains an open question.

Confirming expectations, our results highlight the negligible impact of taking into account versus ignoring dark energy perturbations in the data analysis upon considering the decoupling regime of parametrically large Proca masses. The naive reason why this had to be

¹⁴Foreground effects may also be enhanced by anisotropic stress. However, we have checked that the EPN special model does not introduce anisotropic stress, in full analogy with GP theory [35, 37]; see Appendix A.

Model/Parameters	CMB	CMB + DESI	CMB + DESI + PPS	DESI	PPS
$\Lambda \mathrm{CDM}$					
DIC	5498.05 ± 0.10	5506.94 ± 0.16	6251.24 ± 0.34	8.39 ± 0.06	728.04 ± 0.002
WAIC	5498.95 ± 0.07	5508.29 ± 0.68	6252.01 ± 0.19	8.41 ± 0.09	728.08 ± 0.03
$-\ln B$	5498.59 ± 0.27	5509.75 ± 2.72	6251.25 ± 0.14	8.85 ± 0.10	728.37 ± 0.14
Tension against				CMB	CMB + DESI
$-\ln R$				2.31 ± 2.93	13.12 ± 2.92
Goodness of Fit				$2.53 \pm 0.56\sigma$	$5.65 \pm 0.30\sigma$
Suspiciousness				$2.04 \pm 0.47\sigma$	$5.52 \pm 0.27\sigma$
EPN $M = -1/3$					
$\Delta { m DIC}$	0.42 ± 0.15	0.19 ± 0.33	1.6 ± 0.42	0.51 ± 0.07	0.45 ± 0.07
$\Delta ext{WAIC}$	1.09 ± 0.76	-0.55 ± 0.91	2.2 ± 0.22	0.51 ± 0.16	0.43 ± 0.15
$\Delta - \ln B$	-0.66 ± 2.68	-2.0 ± 3.24	2.24 ± 0.22	0.28 ± 0.30	0.79 ± 0.80
Tension against				CMB	CMB + DESI
$\Delta - \ln R$				-2.41 ± 3.11	3.83 ± 3.22
Δ Goodness of Fit				$-1.23 \pm 0.66\sigma$	$0.70 \pm 0.40\sigma$
Δ Suspiciousness				$-1.01 \pm 0.49 \sigma$	$0.60 \pm 0.35\sigma$
EPN $M = -1/2$					
$\Delta { m DIC}$	1.31 ± 0.23	2.80 ± 0.20	11.85 ± 0.42	1.11 ± 0.15	0.76 ± 0.02
$\Delta ext{WAIC}$	1.56 ± 0.31	2.17 ± 0.87	11.94 ± 0.26	1.11 ± 0.24	0.75 ± 0.04
$\Delta - \ln B$	1.31 ± 1.09	0.28 ± 3.12	13.51 ± 3.01	1.30 ± 0.87	0.94 ± 0.19
Tension against				CMB	CMB + DESI
$\Delta - \ln R$				-2.68 ± 3.40	12.64 ± 4.21
Δ Goodness of Fit				$-0.42 \pm 0.57\sigma$	$1.52 \pm 0.34\sigma$
Δ Suspiciousness				$-0.29 \pm 0.49 \sigma$	$1.51 \pm 0.32 \sigma$
EPN special M					
$\Delta \mathrm{DIC}$	0.53 ± 0.19	-0.35 ± 0.38	-3.2 ± 0.57	0.61 ± 0.07	0.18 ± 0.09
$\Delta \mathrm{WAIC}$	0.45 ± 0.11	-0.62 ± 0.79	-2.4 ± 0.41	0.46 ± 0.10	-0.03 ± 0.12
$\Delta - \ln B$	0.94 ± 2.27	-2.39 ± 3.91	-2.99 ± 1.70	0.82 ± 0.96	-0.18 ± 0.30
Tension against				CMB	CMB + DESI
$\Delta - \ln R$				-4.16 ± 4.28	-0.46 ± 3.99
Δ Goodness of Fit				$-0.64 \pm 0.58 \sigma$	$-0.18 \pm 0.40 \sigma$
Δ Suspiciousness				$-0.87 \pm 0.47 \sigma$	$-0.29 \pm 0.39 \sigma$

Table 4. Analysis information criteria, Goodness of Fit, and Suspiciousness from several data combinations, in Λ CDM and EPN special M models with M=-1/3, M=-1/2 and M as fitting parameter.

the case is that EPN is essentially a theory of dark energy with suppressed early-time modifications to cosmology. However, it is worth noticing that perturbations do lead to significant constraints on model parameters in the context of GP theory [41]. In this regard, the EPN special model may be seen as a particularly motivated theory of dark energy, addressing the late-time cosmic acceleration puzzle while leaving plenty of parameter space left to address cosmological tensions.

4.3 Model comparison

Table 4 shows the results of various IC measures, Goodness of Fit and Suspiciousness obtained for each model and dataset combination. Following the Jeffreys scale (cf. Table 5), we find the special EPN model with M = -1/2 to be ruled out by the CMB + DESI + PPS dataset. On the other hand, the Δ IC values derived from the CMB, DESI, PPS and CMB + DESI datasets show good alignment between Λ CDM and the EPN models with M = -1/3 and with adjustable M, although the former is mildly tensioned when considering combined CMB

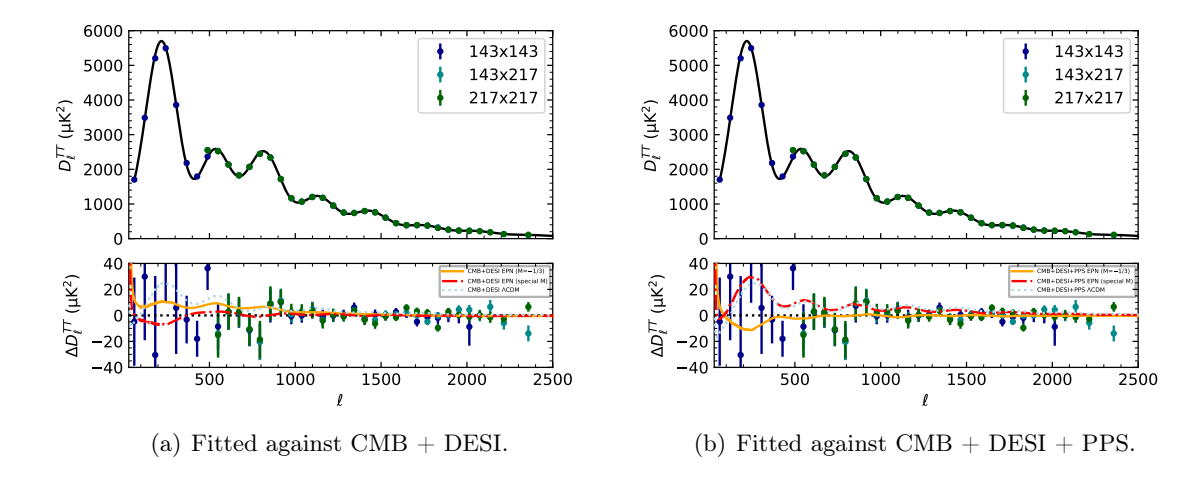


Figure 8. The best-fit CMB TT power spectrum (top panels) and the residue (bottom) against best-fit ΛCDM model TT power spectrum from the CMB dataset. The top panels are identical. Data points were taken from the Planck CamSpec PR4 data release (from Fig. 6 of [1]). The residue plots correspond to the fits against CMB+DESI and CMB+DESI+PPS datasets, respectively. There are evident discrepancies between the fits against CMB data (black dotted line) and both against CMB+DESI and CMB+DESI+PPS datasets in ΛCDM. This tension is alleviated in EPN theory, improving compatibility between CMB and DESI measurements.

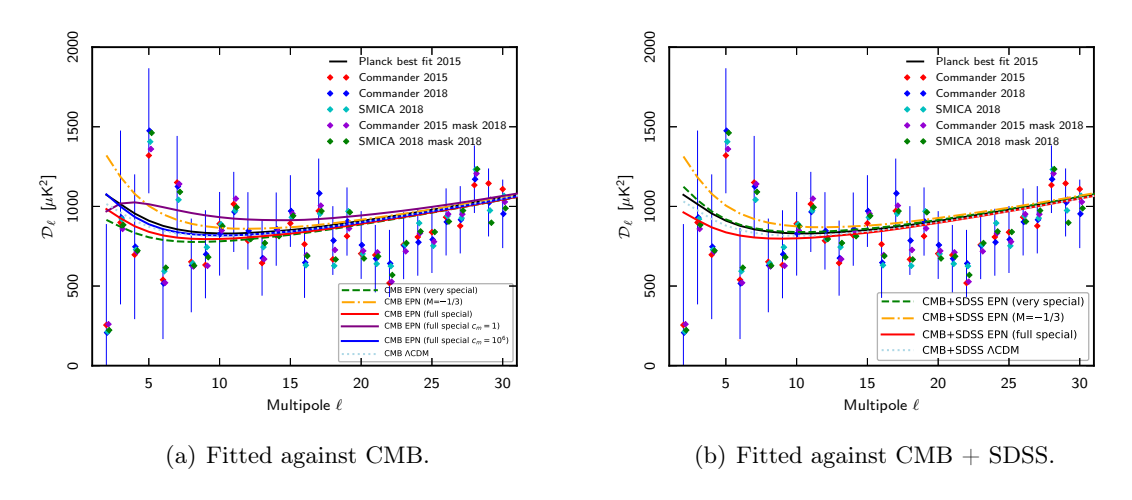


Figure 9. Same as Fig. 8 for CMB TT low- ℓ power spectra. Also shown are data of various maps and masks from the Planck-18 data release (from Fig. 2 of [3]). Black solid line is the best-fit Λ CDM model prediction from Planck-15. The left panel further highlights the effect of the EPN parameter c_m on the low- ℓ spectrum, displaying results either with adjustable c_m (green and red curves, very special and full special models) or with fixed c_m (purple and blue curves, full special model); for the latter, other parameters are chosen to match the best-fit values of the full special model.

+ DESI + PPS data.¹⁵ The CMB + DESI dataset appears to favor both of these models over Λ CDM. Moreover, the tension probes suggest that CMB and DESI data are significantly more compatible in these EPN set-ups than in Λ CDM. The model with M as fitting parameter

¹⁵The favorable alignment between Λ CDM and the special EPN model with M=-1/3 inferred from DESI data is in agreement with the analysis of [58].

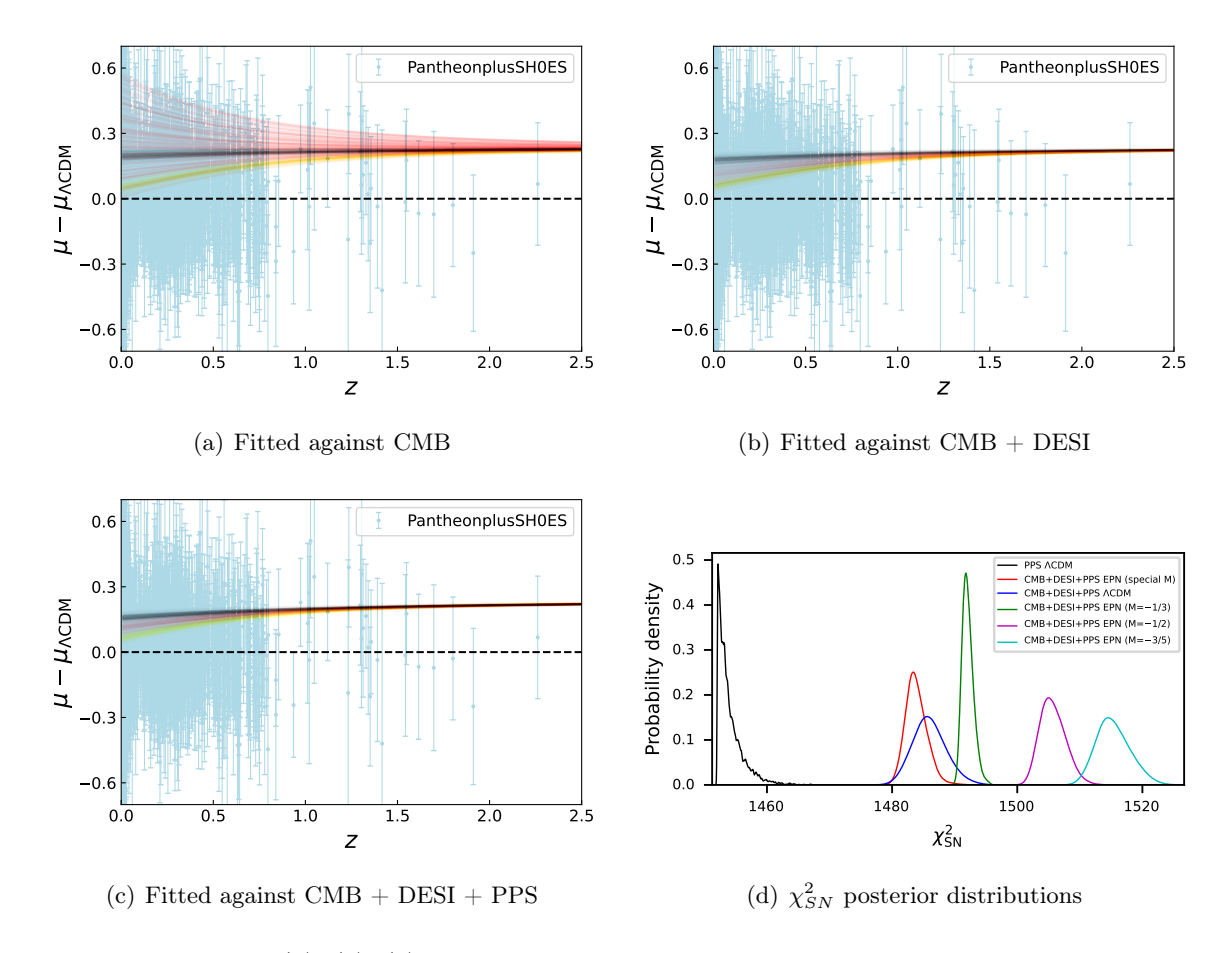


Figure 10. Panels (a), (b), (c): Reconstructed distance modulus fitted against CMB, CMB+DESI and CMB+DESI+PPS datasets in ΛCDM (black), EPN special M model with M=-1/3 (yellow) and EPN special M model with adjustable M (red). The black dashed line in each figure represents the best-fit ΛCDM model from PPS data. Panel (d): The $\chi^2_{\rm SN}$ posterior distributions from PPS in ΛCDM and CMB+DESI+PPS in ΛCDM and four realizations of the EPN special M model (M=-1/3,-1/2,-3/5 and fitting M).

also shows an improved credibility from the CMB + DESI + PPS dataset resulting in a slight alleviation of the tension between CMB + DESI and PPS data.

The improved compatibility between the CMB and DESI datasets can be seen in the CMB power spectra, as shown in the reconstructed high- ℓ TT power spectrum shown in Fig. 8: there are evident discrepancies between the high- ℓ TT power spectra in Λ CDM fitted against CMB data and against CMB + DESI and CMB + DESI + PPS data, which is visibly alleviated in both of these realizations of EPN. For completeness, we also display the low- ℓ TT power spectrum in Fig. 9. It is clear that, as long as $c_m \gg 1$, EPN matches closely with Λ CDM, with a very slight suppression for the lowest ℓ modes. We remark that such a suppression cannot explain the quadruple anomaly [123].

Fig. 10 shows the reconstructed distance modulus obtained from various dataset combinations. The manifest difference between the resulting fits provides an explanation for the tension between CMB + DESI and PPS data. The results for the $\chi^2_{\rm SN}$ distribution also shown again the mild preference of the special EPN model with M as adjustable parameter. Inter-

estingly, while models with fixed M perform worse than Λ CDM in regards to this tension, the more minimal and natural set-up with M=-1/3 shows a strong preference over other theoretically motivated choices.

5 Conclusions

The aim of this work is to evaluate the viability of the vector-tensor EPN theory as a consistent and well-motivated framework of dynamical dark energy and identify whether it may be competitive against the standard Λ CDM model (accounting for an increase in parameter space). Our first observation was that EPN accommodates an interesting one-parameter extension of background cosmology, encompassing the so-called special (minimally coupled) EPN model, particular cases of the general EPN model, as well as other theories such as GP. This extension corresponds to an effective dark energy fluid with density $\rho_{\rm EPN} \propto H^{2M}$, with M a parameter that may be freely adjusted in phenomenological studies such as the present one. On the other hand, it is an appealing feature that such modifications may emerge in EPN theory without the inclusion of operators that are unnatural from an EFT perspective, although it must be recalled that one still needs some degree of fine tuning in order to obtain simple decoupled equations for the background functions. We think our results motivate the analysis of more general parameterizations in future studies, including ones arising from models without any fine-tuning. At the same time, the degeneracy of different theories at the background level motivates the inclusion of perturbations when confronting the predictions of EPN with data. Here we have taken the first step in this direction, by analyzing the fit of the matter power spectrum and structure growth rate, within a particular version of the EPN special model.

The main target of our analysis was to assess whether the EPN theory (or akin theories) can have the potential to address the notorious tensions currently present in cosmological data. We have found that, in a particular realization, the special EPN model results in an easing of the Hubble tension from 5.81σ to 1.52σ , but at the cost of an increase in the $\Omega_{\rm m0}$ tension from 0.85σ to 5.19σ , netting an increase in all tension probes utilized in this work. This is consistent with other thawing phantom models, in particular the CPL phenomenological model with a matching cosmographic equation of state.

Our results also highlight the critical importance of perturbations when confronting the model with current data, improving on previous work that focused exclusively on the background dynamics. We find that 'natural' values of the Proca mass, i.e. $m \sim \Lambda^2/M_{\rm Pl}$, result in significant enhancements of CMB foreground effects. Agreement with data can however be recovered at ever so slightly larger masses, resulting in parameter posteriors, growth history, and matter power spectrum which are similar to the toy set-up where dark energy perturbations are turned off. We emphasize that this regime is acceptable both phenomenologically and theoretically, as it amounts to a mild tuning in only one model parameter. As long as stability criteria are met, this set-up thus provides a consistent description which allows one to isolate the observational effects that result from the modification of the Friedmann equation. This is very pertinent since, as we have emphasized repeatedly, the same class of modification is common to several other dark energy models with vector degrees of freedom. The cosmological fit of this background-only one-parameter special M model shows that it is favored over Λ CDM by 1.5 σ when combining *Planck* datasets with DESI BAO, and by 2.4σ when further adding the PantheonPlus+SH0ES dataset. We also note that our analysis shows no evidence of an upper limit on the allowed value of the mass.

Returning to the full set-up with perturbations, we find that the theoretically motivated very special EPN model also performs better than Λ CDM when comparing the derived S_8 value of the DES Y3 weak lensing dataset with the predicted matter perturbation power at $8 \,\mathrm{Mpc}/h$, thus easing the S_8 tension. However, when analyzing the complete matter power spectrum, we notice a strong enhancement at the BAO scale, in conflict with the full-shape analysis of the SDSS galaxy clustering dataset. This large-scale matter power enhancement, which cannot be captured by σ_8 , may therefore be seen as an important metric for assessing the viability of EPN theories beyond the background level. The growth history of this particular model is also marginally different from that of Λ CDM. In combination, the large-scale structure dataset may serve as a consistency check for EPN theory and motivates follow-up research on more general EPN models fully including perturbations.

In conclusion, we have found that EPN theory restricted to a one-parameter subclass of models performs marginally better than ΛCDM , although at the price of a mild tuning of parameters which suppresses the effect of dark energy perturbations. Moreover, it is clear that this particular framework is unsuccessful at resolving all cosmological tensions, yet we find our results to be promising enough to warrant further studies that include a wider parameter space, which could investigate the possibility of additional mechanisms for altering the evolution of matter perturbations and potentially address the aforementioned tensions.

Acknowledgments

We would like to thank Lavinia Heisenberg for useful discussions. The work of HWC, SGS and XZ was partly supported by the NSFC (Grant No. 12250410250). The work of CdR is supported by STFC Consolidated Grant ST/X000575/1. CdR is also supported by a Simons Investigator award 690508. SGS also acknowledges support from a Provincial Grant (Grant No. 2023QN10X389).

A Initial conditions, effective Newton constant, and anisotropic stress

A.1 Adiabatic initial conditions

To perform the numerical integration of the perturbation equations in CAMB we adopt the standard choice of adiabatic initial conditions. The task is therefore to identify the adiabatic modes for the EPN system considered in this paper. To this end, and in what follows, it proves convenient to introduce the gauge-invariant quantity

$$\delta_{B,i} \equiv \frac{\delta \rho_i}{\rho_i} + \frac{3H}{M_{\rm Pl}^2} (1 + w_i) v_i \,, \tag{A.1}$$

for each matter species i, as well as the rescaled (dimensionless) variables

$$\tilde{\psi} \equiv \frac{H}{\Lambda \phi} \psi \,, \qquad \tilde{\mathcal{Y}} \equiv \frac{1}{M_{\text{Pl}}^2 \Lambda^2 \Omega_{\text{EPN}}} \hat{\mathcal{Y}} \,.$$
 (A.2)

One advantage is that the master equations for these variables, when expressed in terms of conformal time, depend only on the ratio between the comoving wavenumber and the horizon scale, k/(aH), and do not contain poles at the radiation, matter, or de Sitter fixed points, allowing us to unambiguously and properly define the sub-horizon and super-horizon modes in each era.

To a good approximation, we may simplify the system by assuming a matter sector composed of cold dark matter 'c' and radiation 'r'. In this set-up one may easily identify the only mode (with degeneracy two) that is non-decaying before the dark energy-dominated era $(\Omega_{\rm EPN} \to 0)$. We expect these results to be applicable to the four-fluid system (which also includes baryons and neutrinos) implemented in CAMB.

We write the perturbation equations as a first order matrix system in the basis $\{\delta_{B,c}, \delta_{F,c}, \delta_{B,r}, \delta_{F,r}, \tilde{\mathcal{Y}}, \tilde{\psi}\}$, where $\delta_{F,i} \equiv \delta \rho_i / \rho_i$ is the density contrast (the subscript stands for 'flat', as this quantity is gauge-dependent and we remind the reader that we are working in the spatially flat gauge). We then find the following set of eigen-modes:

$$E_{c,+} = \begin{pmatrix} \Delta, & 3 + \Delta, & 0, & 4, & 0, & 1 \end{pmatrix},$$

$$E_{c,-} = \begin{pmatrix} \frac{4\Omega_{r}}{\Omega_{c}} + 3 + \Delta, 3 + \Delta, & 0, & 4, & 0, & 1 \end{pmatrix},$$

$$E_{r,\pm} = \begin{pmatrix} 0, & 3, & \frac{1+\Omega_{r}}{2\Omega_{r}} (1 \pm i\omega_{J}) + \frac{\Omega_{c}}{\Omega_{r}} \Delta, 4 + \frac{\Omega_{c}}{\Omega_{r}} \Delta, 0, & 1 \end{pmatrix},$$

$$E_{EPN,\pm} = \begin{pmatrix} 0, & 0, & 0, & 0, & 1, \tilde{\psi}_{EPN,\pm} \end{pmatrix},$$
(A.3)

with respective decay rates (i.e. minus the eigenvalues)

$$\frac{\lambda_n}{H} = \left(0, \frac{3 + \Omega_r}{2}, \frac{1 + \Omega_r}{4} (1 \pm i\omega_J), \frac{1}{4} \left(7 + 3\Omega_r - 2M(3 + \Omega_r)\right) + \sqrt{(5 + \Omega_r)^2 + 4M(1 - \Omega_r)(5 + \Omega_r - M(3 + \Omega_r))\Delta}\right),$$
(A.4)

where $\Delta \equiv \frac{2}{3\Omega_c} \frac{k^2}{a^2 H^2}$ and $\omega_J^2 \equiv k^2/k_J^2 - 1$ measures how much a mode k lies below the Jeans scale $k_J^2 \equiv \frac{3}{16} a^2 H^2 (1 + \Omega_r)^2$. We also introduced

$$\begin{split} \tilde{\psi}_{\mathrm{EPN},\pm} &\equiv -\frac{1}{8M(3+\Omega_{\mathrm{r}}+(1-\Omega_{\mathrm{r}})\Delta)} \bigg[5+\Omega_{\mathrm{r}}+2M(1-\Omega_{\mathrm{r}})\Delta \\ &\pm \sqrt{(5+\Omega_{\mathrm{r}})^2+4M(1-\Omega_{\mathrm{r}})(5+\Omega_{\mathrm{r}}-M(3+\Omega_{\mathrm{r}}))\Delta} \bigg] \,, \end{split} \tag{A.5}$$

On super-horizon scales $(k \ll aH)$ we have $\omega_J \simeq i$ and $\Delta \simeq 0$. We then see that the only frozen modes are $E_{\rm c,+}$ and $E_{\rm r,+}$. In the strict limit k=0, these modes are degenerate and equal to $(0\,,3\,,0\,,4\,,0\,,1)$, which corresponds to the standard adiabatic mode, which sets equal amplitudes for the perturbations $\frac{1}{3}\delta\rho_{\rm c}/\rho_{\rm c}$, $\frac{1}{4}\delta\rho_{\rm r}/\rho_{\rm r}$ (i.e. $\frac{1}{3(1+w_i)}\delta\rho_i/\rho_i$) and $\tilde{\psi}$, with zero $\delta_{B,i}$ and $\tilde{\mathcal{Y}}$. Of course, away from this strict limit, there exists an orthogonal combination, $E_{\rm c,+}-E_{\rm r,+}$, which however has $\delta_{B,\rm c}=\delta_{F,\rm c}$, i.e. $v_{\rm c}=0$. Such mode thus cannot be sourced by the curvature perturbation, which sets $v_i\neq 0$ for all species on super-horizon scales [124].

Having identified the adiabatic mode, we may then match its super-horizon expression to the corresponding one on sub-horizon scales $(k \gg aH)$. We focus on the ratio $\delta_{B,c}/\tilde{\psi}$ of the mode $E_{c,+}$, the advantage being that this quantity is independent of the coupling between photons and baryons, and thus robust in our approximation where we neglect the latter. Thus we conclude that the choice of adiabatic initial conditions is given by $\tilde{\psi} = \Delta^{-1}\delta_{B,c}$ and $\tilde{\mathcal{Y}} = 0$ (with $\delta_{B,c}$ evaluated in synchronous gauge for usage in CAMB).

 $^{^{-16}}$ At this stage we notice an obvious issue with our choice of basis, namely that $\Delta \to \infty$ in the sub-horizon limit, leading to an artificial hierarchy between $E_{\text{EPN},\pm}$ and the rest of the eigen-modes. We can easily remedy this by rescaling $\tilde{\psi}$ and $\tilde{\mathcal{Y}}$ by Δ . This redefinition introduces a mixing between $E_{\text{c},+}$ and $E_{\text{EPN},\pm}$ (but not with the other modes), however this is irrelevant for our purposes since the latter is always decaying (provided the stability criteria are met).

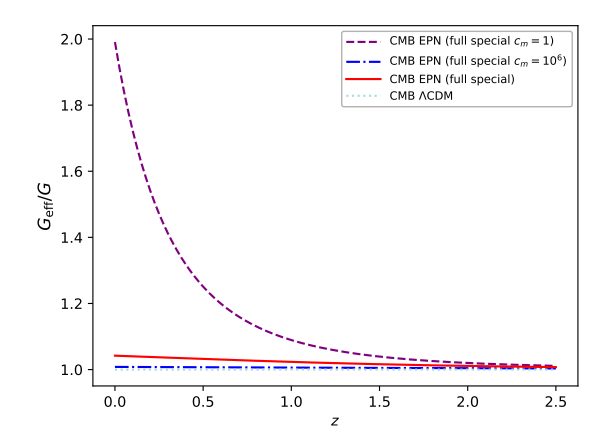


Figure 11. Evolution of the effective Newton constant in the best-fit Λ CDM model and the EPN full special model given the best-fit parameters for the CMB dataset, for different values of the Proca mass parameter c_m , including the best-fit value $c_m = 10^{4.48}$ (red curve). The strong enhancement for $c_m = \mathcal{O}(1)$ values is manifest.

A.2 Effective Newton constant and anisotropic stress

The anisotropic stress Π and effective Newton constant G_{eff} are defined via

$$\Pi \equiv \frac{3a^2}{M_{\rm Pl}^2} \left(\frac{k^i k^j}{k^2} - \frac{1}{3} \delta^{ij} \right) T_{ij} = 2k^2 (\Psi_B + \Phi_B) ,
-2k^2 \Psi_B \equiv \frac{G_{\rm eff}}{G} \frac{a^2}{M_{\rm Pl}^2} \sum_i \rho_i \delta_{B,i} ,$$
(A.6)

where Ψ_B and Φ_B are the Bardeen potentials. In our conventions, these are given in terms of the spatially flat gauge metric perturbations by

$$\Psi_B = \frac{1}{M_{\rm Pl}} \alpha + \frac{1}{M_{\rm Pl}^2} \dot{\chi} \,, \qquad \Phi_B = \frac{H}{M_{\rm Pl}^2} \chi \,.$$
(A.7)

Through some straightforward manipulations of the perturbation equations of Sec. 2.5, we eventually obtain

$$\Pi = \frac{9a^2H^2}{M_{\rm Pl}^2} \sum_{i} \Omega_i \left[3H(c_i^2 - w_i)(1 + w_i) + \dot{w}_i \right] v_i , \qquad (A.8)$$

$$\frac{G_{\text{eff}}}{G} = 1 + \frac{M_{\text{Pl}}^2}{a^2 \sum_i \rho_i \delta_{B,i}} \left(\frac{k^2}{2} \tilde{\mathcal{Y}} - \Pi \right) . \tag{A.9}$$

Given $c_i^2 = w_i = \text{const.}$ under the perfect fluid approximation, we conclude that $\Pi = 0$ and $G_{\text{eff}}/G = 1 + k^2 \tilde{\mathcal{Y}}/(6a^2 H^2 \sum_i \Omega_i \delta_{B,i})$. The vanishing of the anisotropic stress agrees with [35, 37] which derived the same result in the context of GP theory. Fig. 11 displays how G_{eff}/G starts deviating from unity during the matter-dark energy transition, consistent with the adiabatic assumption on the initial conditions, $\tilde{\mathcal{Y}} \to 0$, and the fact that $\tilde{\mathcal{Y}}$ remains frozen prior to the transition.

$\ln B(M_2) - \ln B(M_1), \ln R, \text{ etc.}$	Interpretation
> 5	Strongly disfavored / tensioned
$2.5\sim 5$	Moderately disfavored / tensioned
$1\sim2.5$	Weakly disfavored / tensioned
$-1 \sim 1$	Inconclusive
$-2.5 \sim -1$	Weakly favored / aligned
$-5 \sim -2.5$	Moderately favored / aligned
< -5	Strongly favored / aligned

Table 5. Jeffreys' scale for evaluating the evidence of model M_1 over M_2 or the tension between datasets.

B Information Criteria

The following is a list of the definitions of the information criteria probes utilized in this work:

$$\ln B(D|M) \equiv \ln \int P(D|\theta_M)P(\theta_M)d\theta_M = -\ln V_M - \ln \left\langle \left(P(D|\theta_M)\right)^{-1} \right\rangle_{M|D}, \quad (B.1)$$

$$DIC(D|M) \equiv \ln P(D|\theta_{M,map}) - 2F(D|M), \qquad (B.2)$$

$$WAIC(D|M) \equiv -F(D|M) + BMD(D|M)/2, \tag{B.3}$$

$$F(D|M) \equiv \langle \ln P(D|\theta_M) \rangle_{M|D} \equiv \ln B(D|M) + \text{KL}(D|M), \qquad (B.4)$$

$$BMD(D|M) \equiv 2\left(\left\langle \left(\ln P(D|\theta_M)\right)^2\right\rangle_{M|D} - \left\langle \ln P(D|\theta_M)\right\rangle_{M|D}^2\right), \tag{B.5}$$

$$-\ln R(D_1, D_2|M) \equiv -\ln B(D_1D_2|M) + \ln B(D_1|M) + \ln B(D_2|M),$$
(B.6)

$$GoF(D_1, D_2|M) \equiv -\ln P(D_1D_2|\theta_{M, map}) + \ln P(D_1|\theta_{M, map}) + \ln P(D_2|\theta_{M, map}),$$
 (B.7)

$$S(D_1, D_2|M) \equiv -F(D_1D_2|M) + F(D_1|M) + F(D_2|M). \tag{B.8}$$

Here D and M denote respectively the dataset and the model, and θ_M stands for the model parameters; $P(D|\theta_M)$, $P(\theta_M)$, $P(\theta_M|D) \equiv P(D|\theta_M)P(\theta_M)/B(D|M)$ are the likelihood, prior probability and posterior probability, respectively; $\langle \ldots \rangle_{M|D} \equiv \int (\ldots)P(\theta_M|D)d\theta_M$ is the MCMC mean, $V_M \equiv \int P(\theta_M)d\theta_M$ is the prior volume, F is the deviance, and $\mathrm{KL}(D|M) \equiv \langle \ln P(\theta_M|D) - \ln P(\theta_M) \rangle_{M|D}$ is the Kullback-Leibler divergence; BMD stands for the Bayesian model dimension, and map is the abbreviation of maximum-a-posteriori, i.e. the Bayesian estimate of the model parameters. Our choice of normalization is such that $\ln B$, ICs, $\ln R$, GoF and suspiciousness S all have the same comparative measure as the Bayesian ratio test, i.e. the Jeffreys scale measures; cf. Table 5.

C Full constraint plot of cosmological parameters

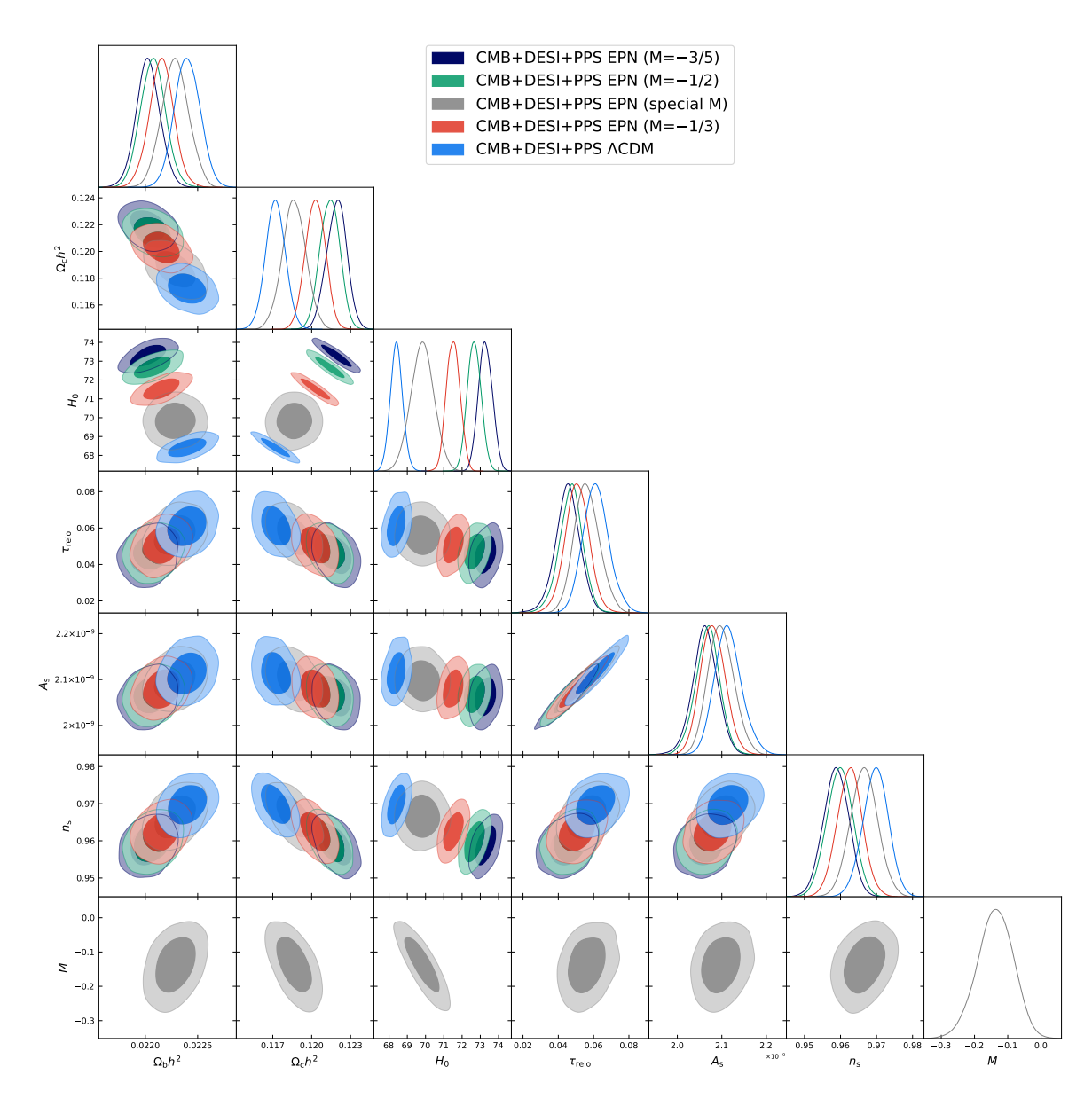


Figure 12. Marginalized posterior constraints on the six base cosmological parameters and special EPN model parameter M, using the CMB+DESI+PPS dataset, in Λ CDM, three EPN models with fixed M, and EPN special M model with unfixed M. Contours indicate 68% and 95% confidence intervals. The resulting constraint on M from this dataset is $M = -0.136^{+0.057}_{-0.051}$ (68% C.L.).

References

- [1] E. Rosenberg, S. Gratton and G. Efstathiou, CMB power spectra and cosmological parameters from Planck PR4 with CamSpec, Mon. Not. Roy. Astron. Soc. 517 (2022) 4620 [2205.10869].
- [2] A.G. Riess et al., A Comprehensive Measurement of the Local Value of the Hubble Constant with 1 km s⁻¹ Mpc⁻¹ Uncertainty from the Hubble Space Telescope and the SH0ES Team, Astrophys. J. Lett. **934** (2022) L7 [2112.04510].
- [3] Planck collaboration, Planck 2018 results. V. CMB power spectra and likelihoods, Astron. Astrophys. 641 (2020) A5 [1907.12875].
- [4] J. Carron, A. Lewis and G. Fabbian, *Planck integrated Sachs-Wolfe-lensing likelihood and the CMB temperature*, *Phys. Rev. D* **106** (2022) 103507 [2209.07395].
- [5] DESI collaboration, DESI 2024 VII: Cosmological Constraints from the Full-Shape Modeling of Clustering Measurements, [2411.12022].
- [6] KILO-DEGREE SURVEY, DES collaboration, DES Y3 + KiDS-1000: Consistent cosmology combining cosmic shear surveys, Open J. Astrophys. 6 (2023) 2305.17173 [2305.17173].
- [7] L. Knox and M. Millea, *Hubble constant hunter's guide*, *Phys. Rev. D* **101** (2020) 043533 [1908.03663].
- [8] E. Di Valentino, O. Mena, S. Pan, L. Visinelli, W. Yang, A. Melchiorri et al., In the realm of the Hubble tension—a review of solutions, Class. Quant. Grav. 38 (2021) 153001 [2103.01183].
- [9] E. Abdalla et al., Cosmology intertwined: A review of the particle physics, astrophysics, and cosmology associated with the cosmological tensions and anomalies, JHEAp 34 (2022) 49 [2203.06142].
- [10] M. Kamionkowski and A.G. Riess, The Hubble Tension and Early Dark Energy, Ann. Rev. Nucl. Part. Sci. 73 (2023) 153 [2211.04492].
- [11] E. Di Valentino et al., The CosmoVerse White Paper: Addressing observational tensions in cosmology with systematics and fundamental physics, [2504.01669].
- [12] W.J. Wolf, C. García-García and P.G. Ferreira, Robustness of dark energy phenomenology across different parameterizations, JCAP 05 (2025) 034 [2502.04929].
- [13] P.G. Ferreira and A. Roskill, A Short Introduction to Cosmology and its Current Status, 9, 2025 [2509.12121].
- [14] W.J. Wolf, C. García-García, T. Anton and P.G. Ferreira, Assessing Cosmological Evidence for Nonminimal Coupling, Phys. Rev. Lett. 135 (2025) 081001 [2504.07679].
- [15] DESI collaboration, DESI 2024 VI: Cosmological Constraints from the Measurements of Baryon Acoustic Oscillations, [2404.03002].
- [16] W.J. Wolf, C. García-García, D.J. Bartlett and P.G. Ferreira, Scant evidence for thawing quintessence, Phys. Rev. D 110 (2024) 083528 [2408.17318].
- [17] L. Huang, R.-G. Cai and S.-J. Wang, The DESI 2024 hint for dynamical dark energy is biased by low-redshift supernovae, [2502.04212].
- [18] G. Efstathiou, Baryon Acoustic Oscillations from a Different Angle, [2505.02658].
- [19] R.R. Caldwell, A Phantom menace?, Phys. Lett. B 545 (2002) 23 [astro-ph/9908168].
- [20] T. Qiu, Y.-F. Cai and X.-M. Zhang, Null Energy Condition and Dark Energy Models, Mod. Phys. Lett. A 23 (2008) 2787 [0710.0115].
- [21] S. Tsujikawa, Quintessence: A Review, Class. Quant. Grav. 30 (2013) 214003 [1304.1961].

- [22] W.J. Wolf, P.G. Ferreira and C. García-García, Cosmological constraints on Galileon dark energy with broken shift symmetry, [2509.17586].
- [23] G. Tasinato, Cosmic Acceleration from Abelian Symmetry Breaking, JHEP **04** (2014) 067 [1402.6450].
- [24] L. Heisenberg, Generalization of the Proca Action, JCAP 05 (2014) 015 [1402.7026].
- [25] M. Hull, K. Koyama and G. Tasinato, Covariantized vector Galileons, Phys. Rev. D 93 (2016) 064012 [1510.07029].
- [26] L. Heisenberg, R. Kase, M. Minamitsuji and S. Tsujikawa, Black holes in vector-tensor theories, JCAP 08 (2017) 024 [1706.05115].
- [27] L. Heisenberg, R. Kase, M. Minamitsuji and S. Tsujikawa, *Hairy black-hole solutions in generalized Proca theories*, *Phys. Rev. D* **96** (2017) 084049 [1705.09662].
- [28] S. Ajith, A. Saffer and K. Yagi, Rotating black holes in valid vector-tensor theories after GW170817, Phys. Rev. D 102 (2020) 064031 [2006.00634].
- [29] F.M. Ramazanoğlu, Spontaneous growth of vector fields in gravity, Phys. Rev. D 96 (2017) 064009 [1706.01056].
- [30] R. Kase, M. Minamitsuji and S. Tsujikawa, Neutron stars with a generalized Proca hair and spontaneous vectorization, Phys. Rev. D 102 (2020) 024067 [2001.10701].
- [31] S. Garcia-Saenz, A. Held and J. Zhang, Destabilization of Black Holes and Stars by Generalized Proca Fields, Phys. Rev. Lett. 127 (2021) 131104 [2104.08049].
- [32] E.S. Demirboğa, A. Coates and F.M. Ramazanoğlu, Instability of vectorized stars, Phys. Rev. D 105 (2022) 024057 [2112.04269].
- [33] H.-W. Chiang, S. Garcia-Saenz and A. Sang, Black hole destabilization via trapped quasinormal modes, Phys. Rev. D 112 (2025) 024017 [2504.04779].
- [34] A. De Felice, L. Heisenberg, R. Kase, S. Mukohyama, S. Tsujikawa and Y.-l. Zhang, Cosmology in generalized Proca theories, JCAP 06 (2016) 048 [1603.05806].
- [35] A. De Felice, L. Heisenberg, R. Kase, S. Mukohyama, S. Tsujikawa and Y.-l. Zhang, Effective gravitational couplings for cosmological perturbations in generalized Proca theories, Phys. Rev. D 94 (2016) 044024 [1605.05066].
- [36] S. Nakamura, R. Kase and S. Tsujikawa, Cosmology in beyond-generalized Proca theories, Phys. Rev. D 95 (2017) 104001 [1702.08610].
- [37] A. de Felice, L. Heisenberg and S. Tsujikawa, Observational constraints on generalized Proca theories, Phys. Rev. D 95 (2017) 123540 [1703.09573].
- [38] C.-Q. Geng, Y.-T. Hsu, J.-R. Lu and L. Yin, A Dark Energy model from Generalized Proca Theory, Phys. Dark Univ. 32 (2021) 100819 [2104.06577].
- [39] A. Savaliya, Dynamical Dark Energy from a Massive Vector Field in Generalized Proca Theory, [2511.01700].
- [40] L. Heisenberg and H. Villarrubia-Rojo, Proca in the sky, JCAP 03 (2021) 032 [2010.00513].
- [41] A. De Felice, C.-Q. Geng, M.C. Pookkillath and L. Yin, Reducing the H_0 tension with generalized Proca theory, JCAP 08 (2020) 038 [2002.06782].
- [42] J. Beltrán Jiménez, C. de Rham and L. Heisenberg, Generalized Proca and its Constraint Algebra, Phys. Lett. B 802 (2020) 135244 [1906.04805].
- [43] C. de Rham and V. Pozsgay, New class of Proca interactions, Phys. Rev. D 102 (2020) 083508 [2003.13773].

- [44] C. de Rham, S. Garcia-Saenz, L. Heisenberg and V. Pozsgay, Cosmology of Extended Proca-Nuevo, JCAP 03 (2022) 053 [2110.14327].
- [45] C. Deffayet, G.R. Dvali and G. Gabadadze, Accelerated universe from gravity leaking to extra dimensions, Phys. Rev. D 65 (2002) 044023 [astro-ph/0105068].
- [46] A. Nicolis, R. Rattazzi and E. Trincherini, The Galileon as a local modification of gravity, Phys. Rev. D 79 (2009) 064036 [0811.2197].
- [47] C. de Rham and G. Gabadadze, Generalization of the Fierz-Pauli Action, Phys. Rev. D 82 (2010) 044020 [1007.0443].
- [48] C. de Rham, G. Gabadadze and A.J. Tolley, Resummation of Massive Gravity, Phys. Rev. Lett. 106 (2011) 231101 [1011.1232].
- [49] C. de Rham, Massive Gravity, Living Rev. Rel. 17 (2014) 7 [1401.4173].
- [50] L. Heisenberg and J. Zosso, Quantum Stability of Generalized Proca Theories, Class. Quant. Grav. 38 (2021) 065001 [2005.01639].
- [51] C. de Rham, L. Heisenberg, A. Kumar and J. Zosso, Quantum stability of a new Proca theory, Phys. Rev. D 105 (2022) 024033 [2108.12892].
- [52] C. de Rham, L. Engelbrecht, L. Heisenberg and A. Lüscher, Positivity bounds in vector theories, JHEP 12 (2022) 086 [2208.12631].
- [53] C. de Rham, J.T. Deskins, A.J. Tolley and S.-Y. Zhou, Graviton Mass Bounds, Rev. Mod. Phys. 89 (2017) 025004 [1606.08462].
- [54] C. de Rham, G. Gabadadze, L. Heisenberg and D. Pirtskhalava, Nonrenormalization and naturalness in a class of scalar-tensor theories, Phys. Rev. D 87 (2013) 085017 [1212.4128].
- [55] C. de Rham, L. Heisenberg and R.H. Ribeiro, Quantum Corrections in Massive Gravity, Phys. Rev. D 88 (2013) 084058 [1307.7169].
- [56] A. Lue and G.D. Starkman, How a brane cosmological constant can trick us into thinking that W < -1, Phys. Rev. D 70 (2004) 101501 [astro-ph/0408246].</p>
- [57] F.K. Anagnostopoulos and E.N. Saridakis, Observational constraints on extended Proca-Nuevo gravity and cosmology, JCAP 04 (2024) 051 [2312.15483].
- [58] L. Sudharani, N.S. Kavya and V. Venkatesha, Unveiling the effects of coupling extended Proca-Nuevo gravity on cosmic expansion with recent observations, Mon. Not. Roy. Astron. Soc. 535 (2024) 1998 [2412.02707].
- [59] L. Heisenberg, R. Kase and S. Tsujikawa, Cosmology in scalar-vector-tensor theories, Phys. Rev. D 98 (2018) 024038 [1805.01066].
- [60] C. Becker, C. Arnold, B. Li and L. Heisenberg, Proca-stinated cosmology. Part I. A N-body code for the vector Galileon, JCAP 10 (2020) 055 [2007.03042].
- [61] S.D.B. Fell and L. Heisenberg, Proca in an Expanding Universe, Fortsch. Phys. 72 (2024) 2400110 [2406.11299].
- [62] L. Bohnenblust, S. Giardino, L. Heisenberg and N. Nussbaumer, To bounce or not to bounce in generalized Proca theory and beyond, JHEP 07 (2025) 124 [2412.03977].
- [63] N.S. Kavya, L. Sudharani and V. Venkatesha, Constraining extended Proca-Nuevo theory through big bang nucleosynthesis, Gen. Rel. Grav. 57 (2025) 53.
- [64] A.M. Sultan, Gravitational Baryogenesis in Extended Proca-Nuevo Gravity, [2504.06133].
- [65] J. Carron, M. Mirmelstein and A. Lewis, CMB lensing from Planck PR4 maps, JCAP 09 (2022) 039 [2206.07773].

- [66] DESI collaboration, DESI 2024 IV: Baryon Acoustic Oscillations from the Lyman alpha forest, JCAP 01 (2025) 124 [2404.03001].
- [67] DESI collaboration, DESI 2024 III: Baryon Acoustic Oscillations from Galaxies and Quasars, [2404.03000].
- [68] D. Brout et al., The Pantheon+ Analysis: Cosmological Constraints, Astrophys. J. 938 (2022) 110 [2202.04077].
- [69] EBOSS collaboration, The 16th Data Release of the Sloan Digital Sky Surveys: First Release from the APOGEE-2 Southern Survey and Full Release of eBOSS Spectra, Astrophys. J. Suppl. 249 (2020) 3 [1912.02905].
- [70] A.J. Ross, L. Samushia, C. Howlett, W.J. Percival, A. Burden and M. Manera, The clustering of the SDSS DR7 main Galaxy sample – I. A 4 per cent distance measure at z = 0.15, Mon. Not. Roy. Astron. Soc. 449 (2015) 835 [1409.3242].
- [71] F. Beutler, C. Blake, M. Colless, D.H. Jones, L. Staveley-Smith, G.B. Poole et al., The 6dF Galaxy Survey: $z \approx 0$ measurement of the growth rate and σ_8 , Mon. Not. Roy. Astron. Soc. 423 (2012) 3430 [1204.4725].
- [72] C.D. Kreisch and E. Komatsu, Cosmological Constraints on Horndeski Gravity in Light of GW170817, JCAP 12 (2018) 030 [1712.02710].
- [73] J. Noller and A. Nicola, Cosmological parameter constraints for Horndeski scalar-tensor gravity, Phys. Rev. D 99 (2019) 103502 [1811.12928].
- [74] A. Spurio Mancini, F. Köhlinger, B. Joachimi, V. Pettorino, B.M. Schäfer, R. Reischke et al., KiDS + GAMA: constraints on horndeski gravity from combined large-scale structure probes, Mon. Not. Roy. Astron. Soc. 490 (2019) 2155 [1901.03686].
- [75] B. Bayarsaikhan, S. Koh, E. Tsedenbaljir and G. Tumurtushaa, Constraints on dark energy models from the Horndeski theory, JCAP 11 (2020) 057 [2005.11171].
- [76] D. Traykova, E. Bellini, P.G. Ferreira, C. García-García, J. Noller and M. Zumalacárregui, Theoretical priors in scalar-tensor cosmologies: Shift-symmetric Horndeski models, Phys. Rev. D 104 (2021) 083502 [2103.11195].
- [77] S. Capozziello, R. De Ritis, C. Rubano and P. Scudellaro, Noether symmetries in cosmology, Riv. Nuovo Cim. 19N4 (1996) 1.
- [78] M. Amarzguioui, O. Elgaroy, D.F. Mota and T. Multamaki, Cosmological constraints on f(r) gravity theories within the palatini approach, Astron. Astrophys. **454** (2006) 707 [astro-ph/0510519].
- [79] M. Benetti, S. Capozziello and G. Lambiase, Updating constraints on f(T) teleparallel cosmology and the consistency with Big Bang Nucleosynthesis, Mon. Not. Roy. Astron. Soc. 500 (2020) 1795 [2006.15335].
- [80] S. Kumar, R.C. Nunes and P. Yadav, New cosmological constraints on f(T) gravity in light of full Planck-CMB and type Ia supernovae data, Phys. Rev. D 107 (2023) 063529 [2209.11131].
- [81] J. Beltrán Jiménez, L. Heisenberg, T.S. Koivisto and S. Pekar, Cosmology in f(Q) geometry, Phys. Rev. D 101 (2020) 103507 [1906.10027].
- [82] S. Wang, Y. Wang and M. Li, Holographic Dark Energy, Phys. Rept. 696 (2017) 1 [1612.00345].
- [83] G. Dvali and M.S. Turner, Dark Energy as a Modification of the Friedmann Equation, [astro-ph/0301510].
- [84] P. Binetruy, C. Deffayet and D. Langlois, Nonconventional cosmology from a brane universe, Nucl. Phys. B 565 (2000) 269 [hep-th/9905012].

- [85] P. Binetruy, C. Deffayet, U. Ellwanger and D. Langlois, *Brane cosmological evolution in a bulk with cosmological constant*, *Phys. Lett. B* **477** (2000) 285 [hep-th/9910219].
- [86] C. Deffayet, Cosmology on a brane in Minkowski bulk, Phys. Lett. B 502 (2001) 199 [hep-th/0010186].
- [87] LIGO SCIENTIFIC, VIRGO, FERMI-GBM, INTEGRAL collaboration, Gravitational Waves and Gamma-rays from a Binary Neutron Star Merger: GW170817 and GRB 170817A, Astrophys. J. Lett. 848 (2017) L13 [1710.05834].
- [88] C. de Rham and S. Melville, Gravitational Rainbows: LIGO and Dark Energy at its Cutoff, Phys. Rev. Lett. 121 (2018) 221101 [1806.09417].
- [89] I. Harry and J. Noller, Probing the speed of gravity with LVK, LISA, and joint observations, Gen. Rel. Grav. 54 (2022) 133 [2207.10096].
- [90] T. Baker, E. Barausse, A. Chen, C. de Rham, M. Pieroni and G. Tasinato, Testing gravitational wave propagation with multiband detections, JCAP 03 (2023) 044 [2209.14398].
- [91] A. Lewis, A. Challinor and A. Lasenby, Efficient computation of CMB anisotropies in closed FRW models, Astrophys. J. 538 (2000) 473 [astro-ph/9911177].
- [92] C. Howlett, A. Lewis, A. Hall and A. Challinor, CMB power spectrum parameter degeneracies in the era of precision cosmology, JCAP 1204 (2012) 027 [1201.3654].
- [93] VIRGO CONSORTIUM collaboration, Stable clustering, the halo model and nonlinear cosmological power spectra, Mon. Not. Roy. Astron. Soc. **341** (2003) 1311 [astro-ph/0207664].
- [94] U. Seljak, Analytic model for galaxy and dark matter clustering, Mon. Not. Roy. Astron. Soc. 318 (2000) 203 [astro-ph/0001493].
- [95] A. Mead, S. Brieden, T. Tröster and C. Heymans, hmcode-2020: improved modelling of non-linear cosmological power spectra with baryonic feedback, Mon. Not. Roy. Astron. Soc. 502 (2021) 1401 [2009.01858].
- [96] W. Hu and N. Sugiyama, Small scale cosmological perturbations: An Analytic approach, Astrophys. J. 471 (1996) 542 [astro-ph/9510117].
- [97] J. Torrado and A. Lewis, Cobaya: Code for Bayesian Analysis of hierarchical physical models, JCAP 05 (2021) 057 [2005.05290].
- [98] A. Lewis and S. Bridle, Cosmological parameters from CMB and other data: A Monte Carlo approach, Phys. Rev. D 66 (2002) 103511 [astro-ph/0205436].
- [99] A. Lewis, Efficient sampling of fast and slow cosmological parameters, Phys. Rev. D 87 (2013) 103529 [1304.4473].
- [100] R.M. Neal, Taking Bigger Metropolis Steps by Dragging Fast Variables, arXiv Mathematics e-prints (2005) math/0502099 [math/0502099].
- [101] A. Lewis, GetDist: a Python package for analysing Monte Carlo samples, [1910.13970].
- [102] F. Avila, A. Bernui, A. Bonilla and R.C. Nunes, Inferring $S_8(z)$ and $\gamma(z)$ with cosmic growth rate measurements using machine learning, Eur. Phys. J. C 82 (2022) 594 [2201.07829].
- [103] EBOSS collaboration, The Completed SDSS-IV extended Baryon Oscillation Spectroscopic Survey: measurement of the BAO and growth rate of structure of the luminous red galaxy sample from the anisotropic correlation function between redshifts 0.6 and 1, Mon. Not. Roy. Astron. Soc. 500 (2020) 736 [2007.08993].
- [104] S.J. Turnbull, M.J. Hudson, H.A. Feldman, M. Hicken, R.P. Kirshner and R. Watkins, Cosmic flows in the nearby universe from Type Ia Supernovae, Mon. Not. Roy. Astron. Soc. 420 (2012) 447 [1111.0631].

- [105] I. Achitouv, C. Blake, P. Carter, J. Koda and F. Beutler, Consistency of the growth rate in different environments with the 6-degree Field Galaxy Survey: Measurement of the void-galaxy and galaxy-galaxy correlation functions, Phys. Rev. D 95 (2017) 083502 [1606.03092].
- [106] M. Feix, A. Nusser and E. Branchini, Growth Rate of Cosmological Perturbations at $z\sim0.1$ from a New Observational Test, Phys. Rev. Lett. 115 (2015) 011301 [1503.05945].
- [107] BOSS collaboration, The clustering of galaxies in the completed SDSS-III Baryon Oscillation Spectroscopic Survey: cosmological analysis of the DR12 galaxy sample, Mon. Not. Roy. Astron. Soc. 470 (2017) 2617 [1607.03155].
- [108] BOSS collaboration, The clustering of galaxies in the SDSS-III Baryon Oscillation Spectroscopic Survey: cosmological implications of the full shape of the clustering wedges in the data release 10 and 11 galaxy samples, Mon. Not. Roy. Astron. Soc. 440 (2014) 2692 [1312.4854].
- [109] C. Blake et al., The Wiggle Z Dark Energy Survey: Joint measurements of the expansion and growth history at z < 1, Mon. Not. Roy. Astron. Soc. 425 (2012) 405 [1204.3674].
- [110] S. Nadathur, P.M. Carter, W.J. Percival, H.A. Winther and J. Bautista, Beyond BAO: Improving cosmological constraints from BOSS data with measurement of the void-galaxy cross-correlation, Phys. Rev. D 100 (2019) 023504 [1904.01030].
- [111] BOSS collaboration, The clustering of galaxies in the SDSS-III Baryon Oscillation Spectroscopic Survey: single-probe measurements from CMASS anisotropic galaxy clustering, Mon. Not. Roy. Astron. Soc. 461 (2016) 3781 [1312.4889].
- [112] M.J. Wilson, Geometric and growth rate tests of General Relativity with recovered linear cosmological perturbations, Ph.D. thesis, Edinburgh U., 2017. 1610.08362.
- [113] EBOSS collaboration, The clustering of the SDSS-IV extended Baryon Oscillation Spectroscopic Survey DR14 quasar sample: a tomographic measurement of cosmic structure growth and expansion rate based on optimal redshift weights, Mon. Not. Roy. Astron. Soc. 482 (2019) 3497 [1801.03043].
- [114] T. Okumura et al., The Subaru FMOS galaxy redshift survey (FastSound). IV. New constraint on gravity theory from redshift space distortions at $z \sim 1.4$, Publ. Astron. Soc. Jap. 68 (2016) 38 [1511.08083].
- [115] B.A. Reid et al., Cosmological Constraints from the Clustering of the Sloan Digital Sky Survey DR7 Luminous Red Galaxies, Mon. Not. Roy. Astron. Soc. 404 (2010) 60 [0907.1659].
- [116] EBOSS collaboration, The one-dimensional power spectrum from the SDSS DR14 Lyα forests, JCAP 07 (2019) 017 [1812.03554].
- [117] S. Watanabe, A widely applicable bayesian information criterion, J. Mach. Learn. Res. 14 (2013) 867–897.
- [118] DES collaboration, Assessing tension metrics with dark energy survey and Planck data, Mon. Not. Roy. Astron. Soc. 505 (2021) 6179 [2012.09554].
- [119] M. Raveri, G. Zacharegkas and W. Hu, Quantifying concordance of correlated cosmological data sets, Phys. Rev. D 101 (2020) 103527 [1912.04880].
- [120] W. Handley and P. Lemos, Quantifying dimensionality: Bayesian cosmological model complexities, Phys. Rev. D 100 (2019) 023512.
- [121] G. Alestas, L. Kazantzidis and L. Perivolaropoulos, H_0 tension, phantom dark energy, and cosmological parameter degeneracies, Phys. Rev. D 101 (2020) 123516 [2004.08363].
- [122] S. Chabanier, M. Millea and N. Palanque-Delabrouille, Matter power spectrum: from Lyα forest to CMB scales, Mon. Not. Roy. Astron. Soc. 489 (2019) 2247 [1905.08103].

- [123] Planck collaboration, Planck 2018 results. VII. Isotropy and Statistics of the CMB, Astron. Astrophys. 641 (2020) A7 [1906.02552].
- [124] S. Weinberg, *Adiabatic modes in cosmology*, *Phys. Rev. D* **67** (2003) 123504 [astro-ph/0302326].